AEDC-TR-77-78

cy.2

NUMERICAL COMPUTATION OF SUBSONIC CONICAL

DIFFUSER FLOWS WITH NONUNIFORM

TURBULENT INLET CONDITIONS

J. C. CHIEN

ENGINE TEST FACILITY
ARNOLD ENGINEERING DEVELOPMENT CENTER
AIR FORCE SYSTEMS COMMAND
ARNOLD AIR FORCE STATION, TENNESSEE 37389

September 1977

Final Report for Period October 1976 — May 1977

Approved for public release; distribution unlimited.

Prepared for

DIRECTORATE OF TEST ENGINEERING
DEPUTY FOR OPERATIONS
ARNOLD ENGINEERING DEVELOPMENT CENTER
AIR FORCE SYSTEMS COMMAND
ARNOLD AIR FORCE STATION, TENNESSEE 37389

This report has been reviewed by the Information Office (OI) and is releasable to the National Technical Information Service (NTIS). At NTIS, it will be available to the general public, including foreign nations.

APPROVAL STATEMENT

This technical report has been reviewed and is approved for publication.

FOR THE COMMANDER

MARION L. LASTER
Director of Test Engineering
Deputy for Operations

ALAN L. DEVEREAUX
Colonel, USAF
Deputy for Operations

UNCLASSIFIED

REPORT DOCUMENTATION PAGE		READ INSTRUCTIONS BEFORE COMPLETING FORM
1 REPORT NUMBER AEDC-TR-77-78	2 GOVT ACCESSION NO.	3 RECIPIENT'S CATALOG NUMBER
4 TITLE (and Subtitle) NUMERICAL COMPUTATION OF SUBSONIC CONICAL DIFFUSER FLOWS WITH NONUNIFORM TURBULENT INLET CONDITIONS		5 TYPE OF REPORT & PERIOD COVERED Final Report—October 1976 – May 1977
		6. PERFORMING ORG. REPORT NUMBER
7 AUTHOR(s) J. C. Chien, ARO, Inc.		8 CONTRACT OR GRANT NUMBER(s)
9 PERFORMING ORGANIZATION NAME AND ADDRESS Arnold Engineering Development Center Air Force Systems Command Arnold Air Force Station, Tennessee 37389		10 PROGRAM ELEMENT, PROJECT, TASK AREA & WORK UNIT NUMBERS Program Element 65807F
11 CONTROLLING OFFICE NAME AND ADDRESS Arnold Engineering Development Center (XRFIS) Arnold Air Force Station, Tennessee 37389		12. REPORT DATE September 1977
		13 NUMBER OF PAGES 73
14 MONITORING AGENCY NAME & ADDRESS(if different from Controlling Office)		15 SECURITY CLASS. (of this report) UNCLASSIFIED
		15a DECLASSIFICATION/DOWNGRADING SCHEDULE N/A

16 DISTRIBUTION STATEMENT (of this Report)

Approved for public release; distribution unlimited.

17. DISTRIBUTION STATEMENT (of the abstract entered in Block 20, if different from Report)

18 SUPPLEMENTARY NOTES

Available in DDC

19 KEY WORDS (Continue on reverse side if necessary and identify by block number)

computations	inlets	Reynolds number
subsonic flow	nonuniform flow	
turbulent flow	models	
diffusers	turbulence	

20. ABSTRACT (Continue on reverse side if necessary and identify by block number)

    Numerical solutions of the Navier-Stokes equations are obtained and results presented for conical diffuser flows with turbulent nonuniform inlet conditions. The turbulent flow field is described by a two-equation, low-Reynolds-number $k-\epsilon$ model with a new turbulence model for axisymmetric flow. Fast convergence is achieved with an improved initial flow-field guess

DD FORM 1473 EDITION OF 1 NOV 65 IS OBSOLETE
1 JAN 73

UNCLASSIFIED

20. ABSTRACT (Continued)

and a multiple grid Gauss-Seidel iteration method. Comparisons
are made with existing data for several diffuser divergence
angles with and without flow separation. Good agreement was
obtained between theory and experiment.

AFSC
Arnold AFS Tenn

PREFACE

The work reported herein was conducted by the Arnold Engineering Development Center (AEDC), Air Force Systems Command (AFSC), under Program Element 65807F. The results were obtained by ARO, Inc., AEDC Division (a Sverdrup Corporation Company), operating contractor for the AEDC, AFSC, Arnold Air Force Station, Tennessee. The work was done under ARO Project No. R33A-03A. The author of this report is J. C. Chien, ARO, Inc. Elton R. Thompson is the Air Force project manager. The manuscript (ARO Control No. ARO-ETF-TR-77-44) was submitted for publication on June 17, 1977.

CONTENTS

APPENDIX

1.0 INTRODUCTION

Conical diffusers are commonly used in wind tunnels, test facili-
ties, propulsion systems, etc. As the flow moves through the diffuser,
the velocity decreases and the static pressure increases. The amount of
the pressure rise, i.e., the diffuser performance, is strongly influenced
by the diffuser inlet flow conditions and the divergence angle. In
addition, the inlet boundary-layer thickness, the velocity profile, the
inlet Mach number, Reynolds number, and the turbulence intensity all
affect the diffuser performance in such a complicated way that diffuser
design has relied almost solely on empirical data.

Using recent advances in computational fluid dynamics and turbu-
lence modeling, a computational method has been developed for incom-
pressible diffuser flows (Ref. 1). The method allows one to obtain
numerical solutions of the Navier-Stokes equations in finite-difference
form. A two-equation k-ε model is employed for the turbulent flow along
with a sublayer coordinate transformation so that the flow field for the
entire diffuser can be computed for both separated and nonseparated flow
cases.

The purpose of the present study is to further verify the numerical
method developed in Ref. 1 by applying it to a conical diffuser configu-
ration with various inlet boundary-layer conditions. The development of
a two-equation turbulence model suitable for axisymmetric flows, a
multiple grid Gauss-Seidel iteration procedure for faster convergence,
and a series of numerical computations are presented along with compari-
sons with available experimental data.

2.0 GOVERNING EQUATIONS

The basic governing equations for the steady-state incompressible
turbulent flow can be written as:

Continuity Equation:

$$\frac{\partial}{\partial x}(r^{\delta}u) + \frac{\partial}{\partial r}(r^{\delta}v) = 0 \tag{1}$$

X-Momentum Equation:

$$u\frac{\partial u}{\partial x} + v\frac{\partial u}{\partial r} = -\frac{\partial}{\partial x}\left(\frac{p}{\rho}\right) + \left\{2\frac{\partial}{\partial x}\left(\nu\frac{\partial u}{\partial x}\right) - \left(\frac{1}{r}\right)^{\delta} \cdot \frac{\partial}{\partial r}\left[\nu r^{\delta}\left(\frac{\partial v}{\partial x} + \frac{\partial u}{\partial r}\right)\right]\right\}$$

$$- \left\{\frac{\partial}{\partial x}\left(\overline{u'^2}\right) + \left(\frac{1}{r}\right)^{\delta}\frac{\partial}{\partial r}\left(r^{\delta}\,\overline{u'v'}\right)\right\} \tag{2}$$

Y-Momentum Equation:

$$u\frac{\partial v}{\partial x} + v\frac{\partial v}{\partial r} = -\frac{\partial}{\partial r}\left(\frac{p}{\rho}\right) + \left\{2\frac{\partial}{\partial r}\left(\nu\frac{\partial v}{\partial r}\right) + \frac{\partial}{\partial x}\left[\nu\left(\frac{\partial v}{\partial x} + \frac{\partial u}{\partial r}\right)\right]\right.$$

$$\left. + \frac{2\nu\delta}{r}\left(\frac{\partial v}{\partial r} - \frac{v}{r}\right)\right\} - \left\{\left(\frac{1}{r}\right)^{\delta} \cdot \frac{\partial}{\partial r}\left(r^{\delta}\overline{v'^2}\right) + \frac{\partial}{\partial x}\left(\overline{u'v'}\right) - \delta\,\frac{\overline{w'^2}}{r}\right\} \tag{3}$$

The turbulent quantities such as $\overline{u'v'}$ can be written in terms of the mean flow quantities through the eddy viscosity concept as

$$\overline{u'^2} = -2\nu_t\frac{\partial u}{\partial x} + \frac{2}{3}k$$

$$\overline{v'^2} = -2\nu_t\frac{\partial v}{\partial r} + \frac{2}{3}k$$

$$\overline{w'^2} = -2\nu_t\frac{v}{r} + \frac{2}{3}k \tag{4}$$

$$\overline{u'v'} = -\nu_t\left(\frac{\partial u}{\partial r} + \frac{\partial v}{\partial x}\right)$$

where ν_t is the eddy viscosity and k is the turbulent kinetic energy (TKE).

After substituting the eddy viscosity expressions into the momentum equations (Eqs. 2 and 3), one can obtain the vorticity equation through cross differentiation. If one also introduces the stream function concept into the continuity equation, the governing equations can be replaced by the vorticity-stream function formulation as:

Vorticity Equation:

$$\left\{\frac{\partial^2 \Omega}{\partial x^2} - \frac{\partial^2 \Omega}{\partial r^2}\right\} - \frac{1}{(\nu + \nu_t)} \left\{\left(u - 2\frac{\partial \nu_t}{\partial x}\right)\frac{\partial \Omega}{\partial x} + \left[v - 2\frac{\partial \nu_t}{\partial r} - \frac{\delta}{r}(\nu - \nu_t)\right]\frac{\partial \Omega}{\partial r}\right\}$$

$$+ \frac{1}{(\nu + \nu_t)}\left\{\delta\,\Omega\left[\frac{v}{r} + \frac{1}{r}\frac{\partial \nu_t}{\partial r} - \frac{(\nu + \nu_t)}{r^2}\right]\right.$$ (5)

$$\left. + \left(\frac{\partial^2 \nu_t}{\partial x^2} - \frac{\partial^2 \nu_t}{\partial r^2}\right)\left(\frac{\partial v}{\partial x} + \frac{\partial u}{\partial r}\right) + 2\left(\frac{\partial^2 \nu_t}{\partial x \partial r}\right)\left(\frac{\partial v}{\partial r} - \frac{\partial u}{\partial x}\right)\right\} = 0$$

where

$$\Omega \equiv \frac{\partial v}{\partial x} - \frac{\partial u}{\partial r}$$

Stream Function Equation:

$$\left\{\frac{\partial^2 \Psi}{\partial x^2} - \frac{\partial^2 \Psi}{\partial r^2}\right\} - \left(\frac{\delta}{r}\right)\frac{\partial \Psi}{\partial r} + r^\delta \Omega = 0$$ (6)

where

$$u = \left(\frac{1}{r}\right)^\delta \frac{\partial \Psi}{\partial r}$$

$$v = -\left(\frac{1}{r}\right)^\delta \frac{\partial \Psi}{\partial x}$$

A second order pressure equation can also be derived, as shown below.

$$\left\{\frac{\partial^2 p}{\partial x^2} + \frac{\partial^2 p}{\partial r^2}\right\} - \left(\frac{\delta}{r}\right)\frac{\partial p}{\partial r} = \Omega^2 - u\left(\frac{\partial \Omega}{\partial r} + \frac{\delta}{r}\Omega\right) + v\left\{\frac{\partial \Omega}{\partial x}\right\}$$

$$- \left\{\frac{\partial^2}{\partial x^2}\left(\frac{u^2 + v^2}{2}\right) + \frac{\partial^2}{\partial r^2}\left(\frac{u^2 + v^2}{2}\right)\right.$$ (7)

$$\left. + \frac{\delta}{r}\frac{\partial}{\partial r}\left(\frac{u^2 + v^2}{2}\right)\right\}$$

3.0 A TWO-EQUATION, LOW-REYNOLDS-NUMBER k-ϵ TURBULENCE MODEL

The eddy viscosity, ν_t, is calculated through the Prandtl-Kolmogorov formula, i.e.,

$$\nu_t = c_\mu \cdot \frac{k^2}{\epsilon} \tag{8}$$

where the turbulent kinetic energy, k, and its dissipation, ϵ, are obtained from the partial differntial euqations presented below.

Turbulent Kinetic Energy Equation (k):

$$\left\{ \frac{\partial^2 k}{\partial x^2} + \frac{\partial^2 k}{\partial r^2} \right\} - \frac{1}{(\nu + \nu_t)} \left\{ \left[u - \frac{\partial^2 \nu_t}{\partial x} \right] \frac{\partial k}{\partial x} + \left[v - \frac{\partial \nu_t}{\partial r} - \delta \frac{(\nu + \nu_t)}{r} \right] \frac{\partial k}{\partial r} \right\}$$

$$+ \frac{\nu_t}{(\nu + \nu_t)} \left\{ 2 \left[\left(\frac{\partial u}{\partial x} \right)^2 + \left(\frac{\partial v}{\partial r} \right)^2 + \left(\frac{v}{r} \right)^2 \delta \right] + \left(\frac{\partial u}{\partial r} + \frac{\partial v}{\partial x} \right)^2 \right\} \tag{9}$$

$$- \frac{1}{(\nu - \nu_t)} \left\{ \epsilon + 2\nu \frac{k}{y^2} \right\} = 0$$

Turbulent Kinetic Energy Dissipation Equation (ϵ):

$$\left\{ \frac{\partial^2 \epsilon}{\partial x^2} + \frac{\partial^2 \epsilon}{\partial r^2} \right\} - \frac{1}{(\nu + \nu_t/\sigma_\epsilon)} \left\{ \left[u - \frac{\partial}{\partial x} \left(\frac{\nu_t}{\sigma_\epsilon} \right) \right] - \frac{\delta}{r} \left(\frac{\nu_t}{\sigma_\epsilon} \right) \right] \frac{\partial \epsilon}{\partial r} \right\}$$

$$+ C_1 \frac{\nu_t}{(\nu + \nu_t/\sigma_\epsilon)} \left(\frac{\epsilon}{k} \right) \left\{ 2 \left[\left(\frac{\partial u}{\partial x} \right)^2 + \left(\frac{\partial v}{\partial r} \right)^2 \right. \right.$$

$$\left. + \left(\frac{v}{r} \right)^2 \delta \right] + \left(\frac{\partial u}{\partial r} + \frac{\partial v}{\partial x} \right)^2 \right\} \tag{10}$$

$$- C_2 \frac{1}{(\nu + \nu_t/\sigma_\epsilon)} \frac{\epsilon^2}{k} = 0$$

The coefficients used in the present analysis are

$$c_\mu = c_{\mu o} + \Delta c_\mu$$

$$c_{\mu o} = \frac{A}{3 (a + A/b)} \tag{11}$$

$$\Delta c_\mu = -\delta \cdot \left(\frac{v}{r} \right) \left(\frac{k}{\epsilon} \right) \cdot \frac{\sqrt{k}}{u_c}$$

where

$$c_1 = 1.36, \quad c_2 = 1.92 \left[1 - 0.3 \exp.(-R^2)\right]$$

$$\sigma_\epsilon = 1.0$$

$$A = \sqrt{2k} \ \frac{y}{\nu}, \quad R = k^2/(\nu\epsilon) \tag{12}$$

$$a = 1,100, \quad b = 0.27$$

The coefficient $c_{\mu o}$ is related to the two-dimensional (2D) planar flows while the coefficient Δc_μ is attributed to the axisymmetry of the flow. The coefficient Δc_μ can also be written as

$$\Delta c_\mu = + \left(\frac{\partial u}{\partial x} + \frac{\partial v}{\partial r}\right) \left(\frac{k}{\epsilon}\right) \cdot \frac{\sqrt{k}}{u_c} \tag{13}$$

through the use of the continuity equation. Justification for the form of Eqs. (11) and (13) is given in the next section.

4.0 DEVELOPMENT OF THE EDDY VISCOSITY COEFFICIENT, c_μ, FOR AXISYMMETRIC FLOWS

The eddy viscosity coefficient, c_μ, developed in Ref. 1 for 2D flows is

$$c_{\mu o} = \frac{A}{3(a + A/b)} \tag{14}$$

where A, a, and b are given in Eq. (12). The asymptotic value of $c_{\mu o}$ for large A (i.e., away from the wall) is 0.09. When the model given by Eq. (14) is used for conical diffuser flow calculations, it produces a faster centerline velocity decay than that indicated by experiment (Ref. 1). A similar result was observed in the case of a round jet (axisymmetric) with a two-equation k-ε model developed by Launder, Rodi, and Spalding (Refs. 2 and 3).

11

In order to study the effect of $c_{\mu o}$ on the flow-field solution for a diffuser, c_μ was lowered to a value of $(0.56\, c_{\mu o})$ throughout the flow field, where $c_{\mu o}$ is given by Eq. (14). The resulting centerline velocity is shown in Fig. 1. It can be seen that the calculated results using the lower value of c_μ compare well with the experimental data by Okwoubi and Azad (Ref. 4). However, the approach of simply setting $c_\mu = 0.56\, c_{\mu o}$ is not completely acceptable for diffuser flows because it changes not only the flow-field solution but also the inlet condition.

In the study of axisymmetric jet flows, Launder, et al., (Ref. 2) designed a formula for c_μ so that the round jet flow field can be computed reasonably well with a two-equation k-ε model. The model, based on the jet centerline decay, is

$$c_\mu = 0.09 - 0.04f \qquad (15)$$

where

$$f = \left| \frac{YC}{2\Delta u} \left(\frac{du_c}{dx} - \left| \frac{du_c}{dx} \right| \right)^2 \right|^{0.2} \qquad (16)$$

The exponent of 0.2 in Eq. (16) is derived from numerical optimization for the jet flow computation. The main objections to this model are: first, the form of c_μ is somewhat arbitrary, and second, c_μ in Eqs. (15) and (16) is a function of x only, i.e., c_μ is constant in the radial direction. Thus, a new model of c_μ was derived for conical diffuser flows. Note that the new model must also be applicable to axisymmetric jet flows because a jet-like flow can be obtained in a diffuser by increasing the diffuser divergence angle. The requirements for the new model for c_μ are: (1) it must be a simple function of the flow-field variables, (2) it must be a function of both radial (r) and axial (x) coordinates, and (3) it must recover the 2D planar form when the flow is locally two dimensional.

4.1 A NEW c_μ MODEL FOR AXISYMMETRIC FLOWS

The shear stress can be written in terms of the velocity gradient in the Prandtl-Kolmogorov model as

$$\frac{\tau}{\rho} = \nu_1 \left(\frac{\partial u}{\partial y} - \frac{\partial v}{\partial x} \right)$$
$$= c_\mu \frac{k^2}{\epsilon} \left(\frac{\partial u}{\partial v} + \frac{\partial v}{\partial x} \right) \tag{17}$$

Let

$$c_\mu = c_{\mu o} - \Delta c_\mu \tag{18}$$

then

$$\frac{\tau}{\rho} = \left(c_{\mu o} + \Delta c_\mu \right) \frac{k^2}{\epsilon} \left(\frac{\partial u}{\partial y} + \frac{\partial v}{\partial x} \right) \tag{19}$$

where Δc_μ is the correction term for the axisymmetric flows.

Since the $c_{\mu o}$ model works well for both planar and axisymmetric pipe flow, it can be expected that Δc_μ becomes important when $\partial u / \partial x$ is nonzero. To retain the two-dimensional applications of the model, one can relate Δc_μ to $\partial u / \partial x + \partial v / \partial y$ which vanishes in planar cases. Thus for axisymmetric flow,

$$\Delta c_\mu \cdot \left(\frac{\partial u}{\partial x} + \frac{\partial v}{\partial r} \right) = -\frac{v}{r} \cdot \delta \tag{20}$$

The above relation can be written in the dimensionless form by introducing a local velocity scale and a local length scale:

$$\Delta c_\mu = -c_{\mu 1} \frac{v}{r} \cdot \frac{\ell_K}{\Delta u_m} \tag{21}$$

where $c_{\mu 1}$ is a constant, ℓ_K is a turbulent scale, and Δu_m is the characteristic velocity. By equating the length scale ℓ_K to $k^{3/2}/\epsilon$ and taking Δu_m as u_c, Eq. (21) becomes

$$\Delta c_\mu = -c_{\mu 1} \frac{v}{r} \frac{k}{\epsilon} \cdot \frac{\sqrt{k}}{u_c} \tag{22}$$

13

The coefficient $c_{\mu 1}$ could be determined from known distributions of u_c, v and, ℓ_K using Eq. (21). However, since detailed experimental data for the conical diffuser are not available, the constant $c_{\mu 1}$ will be determined from round free-jet data and verified for conical diffuser flows. At the centerline of a round jet, v/r is 0.042 $u_c/r_{1/2}$ (Ref. 5) and the length scale, ℓ_K, is 1.2 $r_{1/2}$. Therefore, one can write Δc_μ as

$$\Delta c_\mu = -c_{\mu 1} \frac{0.042 \, u_c}{r_{1/2}} \cdot \frac{1.2 \, r_{1/2}}{u_c} = -c_{\mu 1} \cdot (0.05) \qquad (23)$$

Rodi's estimate of c_μ at the centerline of a round turbulent jet is about 0.04 (Ref. 3). Therefore, from Eq. (23)

$$c_{\mu 1} = -\frac{\Delta c_\mu}{0.05} = -\frac{c_{\mu o} - 0.04}{0.05} \cong -\frac{0.09 - 0.04}{0.05} = -1.0 \qquad (24)$$

Thus, the final expression for the eddy viscosity coefficient c_μ becomes

$$c_\mu = c_{\mu o} + \Delta c_\mu \qquad (25)$$

where

$$c_{\mu o} = \frac{A}{3 \, (a + A/b)}$$

$$\Delta c_\mu = -\delta \cdot \frac{v}{r} \cdot \frac{k}{\epsilon} \cdot \frac{\sqrt{k}}{u_c}$$

4.2 THE c_μ DISTRIBUTION FOR A ROUND JET

The derived c_μ applies to the round jet flow with the mean radial velocity distribution given by Schlichting's and Tollmien's theories. The predicted c_μ distribution is compared with Rodi's estimated distribution that was obtained from experimental data.

Assuming the length scale variation is small across a round jet, i.e., $\ell_K \approx 1.2 \, r_{1/2}$ and that $c_{\mu o}$ is 0.09, c_μ becomes a function of (v/r) only. From Eq. (25),

$$c_\mu = 0.09 - \left(\frac{v}{r}\right) \cdot \frac{1.2 \, r_{1/2}}{u_c} \qquad (26)$$

$$= 0.09 - 1.2 \frac{(v/u_c)}{(r/r_{1/2})}$$

14

The expression v/u_c can be obtained from either Schlichting's (Ref. 6) or Tollmien's theory (Ref. 7). From Schlichting's theory,

$$v = \frac{1}{4} \sqrt{3/\pi} \; \frac{\sqrt{K}}{x} \; \frac{\eta - \frac{1}{4}\eta^3}{\left(1 + \frac{1}{4}\eta^2\right)^2} \tag{27}$$

where

$$\eta = \frac{1}{4} \sqrt{3/\pi} \; \frac{\sqrt{K}}{\nu_t} \cdot \frac{v}{x} \quad \text{and} \quad u_c = \frac{3}{8\pi} \frac{k}{\nu_t x} \cdot \text{with} \; \frac{\nu_t}{\sqrt{k}} = 0.0161$$

Thus,

$$\frac{v}{u_c} = \frac{0.0322}{\sqrt{3}} \sqrt{\pi} \; \frac{\eta - \frac{1}{4}\eta^3}{\left(1 + \frac{1}{4}\eta^2\right)^2} \tag{28}$$

Also, from Ref. (6),

$$r_{1/2} = 5.27 \frac{x\nu_t}{\sqrt{K}} = (5.27 * 0.0161) \; x$$

and

$$\frac{r}{r_{1/2}} = \frac{1}{(5.27 * 0.0161)} \cdot \frac{r}{x} = \frac{4\sqrt{\pi}}{5.27 \cdot \sqrt{3}} \cdot \eta \tag{29}$$

Substituting Eqs. (28) and (29) into Eq. (26), the final expression for c_μ becomes

$$c_\mu = 0.09 - 0.0424 \; \frac{\left(1 - \frac{1}{4}\eta^2\right)}{\left(1 + \frac{1}{4}\eta^2\right)^2} \tag{30}$$

The c_μ distribution of Eq. (30) is shown in Fig. 2. For large values of η, i.e., at the outer edge of the jet,

$$c_\mu = 0.09 + \frac{0.1696}{\eta^2} \tag{31}$$

Therefore, the asympototic value at $\eta \to \infty$ is 0.09. This is consistent with the flow behavior, because as one moves away from the centerline the factor $(1/r)$ diminishes and the flow behaves more or less like a two-dimensional planar flow. The c_μ distribution obtained with Tollmien's velocity distribution is also shown in Fig. 2. Rodi's estimate

15

of c_μ for a round jet, based on Wygnanski, et al., measurements, is also included for comparison. Although the trend and level of c_μ near the centerline region is roughly the same, the behavior of Rodi's c_μ is quite different from the present theory.

5.0 BOUNDARY CONDITIONS AND COORDINATE TRANSFORMATION

5.1 BOUNDARY CONDITIONS

Boundary conditions for the diffuser flow can be divided into four regions, namely, the inlet condition, the exit condition, the symmetry condition, and the wall condition.

5.1.1 Inlet Boundary Condition

Two types of inlet conditions are used in the present analysis, the fully developed pipe flow inlet condition and a boundary-layer inlet condition with a potential core region.

For the fully developed pipe flow condition, the profile is obtained by solving the three stations in the inlet section of the diffuser until convergence is reached. The convergent pipe flow solution is then held fixed as the inlet condition for the subsequent diffuser flow-field computations. With this condition, the only parameter needed to prescribe the profile is the inlet Reynolds number; all other initial condition parameters, i.e., velocity profiles, TKE profile, etc., are computed and are self-consistent. For a nonfully developed profile, i.e., a boundary layer with a potential core region, prescription of the inlet condition is more involved. Every flow parameter (Ω, u, v, Ψ, k, ε, and ν_t) must be given consistently, not only in the core region but also throughout the sublayer. In the present analysis, the boundary-layer thickness (y_e) is first given and the total shear stress distribution is calculated from

$$\frac{\tau_{tot}}{\rho} = \frac{v^{*2}}{2} \left[1 + \cos\left(\frac{y}{y_e} \cdot \pi\right) \right], \ 0 \leq y \leq y_e \quad \text{(Boundary Layer)}$$
$$\tau_{tot} = 0 \qquad\qquad , \ y > y_e \text{ (Core Region)}$$

(32)

The mixing length distribution is obtained as

$$\ell_m = 0.09 \ \tanh \left(\frac{0.41}{0.09} \ \frac{y}{y_\delta}\right) \cdot y_\delta \tag{33}$$

for both the boundary layer and core regions. Equations (32) and (33) are then used to compute the vorticity distribution through the modified Van Driest formula

$$\Omega^+ = \frac{\partial u^+}{\partial y^+} = \frac{2 \left(\frac{\tau_{tot}}{\tau_w}\right)}{1 + \sqrt{1 + \left[2 \ \ell_m^- \ D\left(\frac{\tau_{tot}}{\tau_w}\right)\right]^2}} \tag{34}$$

where

$$\ell_m^+ = \frac{\ell_m \cdot v^*}{\nu} \ , \ D = \left\{1 - e^{\left(-\frac{y^+}{A^+}\right)}\right\}$$

$$y^+ = \frac{y v^*}{\nu} \ , \ A^+ = 26$$

$$\frac{\tau_w}{\rho} = v^{*2} \ , \ u^- = \frac{u}{v^*}$$

The velocity and the stream function are then obtained from Eq. (34) through a numerical integration scheme. The free-stream values of the turbulent kinetic energy and the eddy viscosity are computed from

$$k_e = \frac{3}{2} \ (k1 \cdot u_{1.c})^2$$

$$\nu_{t,e} = k2 \cdot u_{1,c} \cdot \left(\frac{\delta}{8}\right) \tag{35}$$

where k1 and k2 are free-stream proportionality constants. Typical values for the present analysis are

$$k1 = 0.01 \ \text{and} \ k2 = 0.002 \tag{36}$$

Finally, k and ϵ are computed for the boundary-layer region from

$$\nu_t = \ell_m^2 \cdot \frac{\partial u}{\partial y}$$

$$k = \frac{\nu_t}{0.3} \left(\frac{\partial u}{\partial y}\right) \tag{37}$$

$$\epsilon = c_\mu \cdot \frac{k^2}{\nu_t}$$

5.1.2 Exit Boundary Condition

With a diffuser incorporating a constant area section at the exit (tail pipe), the tail pipe exit boundary condition can be specified by the parallel flow condition, i.e., $\partial/\partial x = 0$.

5.1.3 Symmetry Condition

The symmetry condition is imposed to reduce the computational domain. Along the line of symmetry ($r = 0$), the following conditions are satisfied:

$$
\begin{aligned}
\Psi &= 0 , \\
\frac{\partial u}{\partial r} &= \Omega = 0 , \\
\frac{\partial k}{\partial r} &= \frac{\partial \epsilon}{\partial r} = 0 \\
v &= 0
\end{aligned}
\tag{38}
$$

5.1.4 Wall Boundary Condition

Since both the core region and the sublayer region are solved numerically with the present formulation, the wall boundary condition is applied at $y = 0$ as

$$
\begin{aligned}
\Psi &= \text{constant} , \\
\Omega &= \frac{\partial v}{\partial x} - \frac{\partial u}{\partial y} , \\
\nu_t &= k = \epsilon = 0 , \\
u &= v = 0
\end{aligned}
\tag{39}
$$

5.2 COORDINATE TRANSFORMATION WITH A VARIABLE SUBLAYER STRETCHING

In the present analysis, the governing equations along with the boundary conditions are solved in a transformed rectangular domain. This is achieved by transforming the diffuser geometry into a rectangular domain followed by a sublayer stretching so that adequate resolution can be obtained in the wall layer region, see Fig. 3. The sublayer

stretching is designed to adjust automatically for the sublayer velocity gradient. In addition, the relative number of grid points in the sublayer and the core region can also be varied to compensate for the inlet boundary-layer thickness.

The complete coordinate transformation functions in the core and the sublayer regions are listed below along with the transformation factors.

Core Region Transformation Functions

$$r = S(x) \cdot \left\{ 1 - \left[C \cdot \left[(\bar{r}_{max} - \bar{r}) + g(\bar{r}_{max} - \bar{r} - 1)^2 \right] \right. \right.$$

$$\left. \left. - \ell_n \left[\cosh \left[(\bar{r}_{max} - \bar{r}) + g(\bar{r}_{max} - \bar{r} - 1)^2 - 1 \right] \right] + F \right] \right\} \cdot 0 \le \bar{r} \le \bar{r}_o$$

$$\left(\frac{\partial \bar{r}}{\partial r} \right) = \frac{+1}{S(x) \cdot \left[1 + 2g(\bar{r}_{max} - \bar{r} - 1) \right] \cdot \left\{ C + \tanh \left[(\bar{r}_{max} - \bar{r}) + g(\bar{r}_{max} - \bar{r} - 1)^2 - 1.0 \right] \right\}}$$

$$\left(\frac{\partial^2 \bar{r}}{\partial r^2} \right) = + \left(\frac{\partial \bar{r}}{\partial r} \right)^3 \cdot S(x) \cdot \left\{ 2g \cdot \left[C + \tanh \left[(\bar{r}_{max} - \bar{r}) + g(\bar{r}_{max} - \bar{r} - 1)^2 - 1.0 \right] \right] \right.$$

$$\left. + \left[1 + 2g(\bar{r}_{max} - \bar{r} - 1) \right]^2 \cdot \operatorname{sech}^2 \left[(\bar{r}_{max} - \bar{r}) + g(\bar{r}_{max} - \bar{r} - 1)^2 - 1.0 \right] \right\} \quad (40)$$

$$\left(\frac{\partial^2 \bar{r}}{\partial x^2} \right) = -S'(x) \frac{r}{S(x)} \left(\frac{\partial^2 \bar{r}}{\partial x \partial r} \right) - \left(\frac{\partial \bar{r}}{\partial r} \right) \cdot \left[S''(x) \frac{r}{S(x)} - \left(\frac{S'(x)}{S(x)} \right)^2 \cdot r \right]$$

$$\left(\frac{\partial \bar{r}}{\partial x} \right) = -\left(\frac{\partial \bar{r}}{\partial r} \right) \cdot S'(x) \cdot \frac{r}{S(x)}$$

$$\left(\frac{\partial^2 \bar{r}}{\partial x \partial r} \right) = -\left(\frac{\partial \bar{r}}{\partial x} \right) \cdot \frac{\left(\frac{\partial^2 \bar{r}}{\partial r^2} \right)}{\left(\frac{\partial \bar{r}}{\partial r} \right)} - \frac{S'(x)}{S(x)} \cdot \left(\frac{\partial \bar{r}}{\partial r} \right)$$

Sublayer Region Transformation Function:

$$r = S(x) \left\{ 1 - \frac{\alpha}{\beta} \cdot \tan \beta \left(\tilde{r}_{max} - \tilde{r} \right) \right\} \cdot \tilde{r}_0 \leq \tilde{r} \leq \tilde{r}_{max}$$

$$\frac{\partial \tilde{r}}{\partial r} = \frac{1}{\alpha \cdot S(x)} \cos^2 \left[\beta \left(\tilde{r}_{max} - \tilde{r} \right) \right]$$

$$\frac{\partial \tilde{r}}{\partial x} = -\left(\frac{\partial \tilde{r}}{\partial r} \right) \cdot S'(x) \cdot \frac{r}{S(x)}$$

$$\frac{\partial^2 \tilde{r}}{\partial r^2} = \frac{2\beta}{\alpha \cdot S(x)} \cdot \left(\frac{\partial \tilde{r}}{\partial r} \right) \cdot \cos \left[\beta \left(\tilde{r}_{max} - \tilde{r} \right) \right] \cdot \sin \left[\beta \left(\tilde{r}_{max} - \tilde{r} \right) \right]$$

$$\frac{\partial^2 \tilde{r}}{\partial x^2} = -\frac{S'(x)}{S(x)} \left(\frac{\partial \tilde{r}}{\partial x} \right) + 2\beta \cdot \tan \left[\beta \left(\tilde{r}_{max} - \tilde{r} \right) \right] \left(\frac{\partial \tilde{r}}{\partial x} \right)^2 \qquad (41)$$

$$- \left(\frac{\partial \tilde{r}}{\partial r} \right) \cdot \left\{ S''(x) \frac{r}{S(x)} - \left(\frac{S'(x)}{S(x)} \right)^2 \cdot r \right\}$$

$$\frac{\partial^2 \tilde{r}}{\partial x \partial r} = \frac{2\beta}{\alpha \cdot S(x)} \cdot \cos \left[\beta \left(\tilde{r}_{max} - \tilde{r} \right) \right] \left(\frac{\partial \tilde{r}}{\partial x} \right) \sin \left[\beta \left(\tilde{r}_{max} - \tilde{r} \right) \right]$$

$$- \frac{S'(x)}{S(x)} \cdot \left(\frac{\partial \tilde{r}}{\partial r} \right)$$

where α, β, c, g and F are coefficients of transformation (Ref. 1). These coefficients are determined through a matching procedure at location $\tilde{r}_0$ (which is set equal to unity in the present analysis). By selecting the proper value of $\tilde{r}_{max}$ (which must be greater than $\tilde{r}_0$), one can adjust the relative number of grid points in the sublayer and the core region. For example, with $\tilde{r}_0 = 1$ and $\tilde{r}_{max} = 2$, there will be 50 percent of the grid points in both the sublayer ($\tilde{r}_0 \leq \tilde{r} \leq \tilde{r}_{max}$) and the core ($0 \leq \tilde{r} \leq \tilde{r}_0$) regions.

6.0 NUMERICAL METHODS

6.1 A GENERAL FINITE DIFFERENCE FORMULATION WITH DECAY FUNCTIONS

The governing equations in the transformed plane $(\tilde{x}, \tilde{r})$ can be written in a standard form as

$$\left\{ a_1 \frac{\partial^2 \phi}{\partial \tilde{x}^2} + a_2 \frac{\partial^2 \phi}{\partial \tilde{r}^2} \right\} - \left\{ b_1 \frac{\partial \phi}{\partial \tilde{x}} + b_2 \frac{\partial \phi}{\partial \tilde{r}} \right\} + d = 0 \qquad (42)$$

where ϕ represents the flow variables Ω, Ψ, k, and ε. The coefficients a_1, a_2, b_1, b_2, and d are given in Appendix A. The general finite difference formulation of Eq. (42) is

$$\left(\frac{a_1}{G_i}\right)\left\{\frac{\phi_{i+1,j} - 2\phi_{i,j} + \phi_{i-1,j}}{\delta\bar{x}^2} - \left(\frac{b_1}{a_1}G_i\right)\frac{\phi_{i+1,j} - \phi_{i-1,j}}{2\delta\bar{x}}\right\}$$
$$+ \left(\frac{a_2}{G_j}\right)\left\{\frac{\phi_{i,j+1} - 2\phi_{i,j} - \phi_{i,i-1}}{\delta\bar{r}^2} - \left(\frac{b_2}{a_2}G_j\right)\frac{\phi_{i,j-1} - \phi_{i,j-1}}{2\delta\bar{r}}\right\} + d_{i,j} = 0 \quad (43)$$

where the decay functions G_i and G_j are evaluated locally as

$$G = 1.0 - 0.0625\,(R)^2 \cdot |R| \leq 2$$
$$= \frac{2}{|R|} - \frac{1}{R^2} \cdot |R| > 2$$

$$\text{where } G = G_i \cdot \text{when } R = \frac{b_1}{a_1} \cdot \delta\bar{x}$$

$$\text{and } G = G_j \cdot \text{when } R = \frac{b_2}{a_2} \cdot \delta\bar{r}$$

(44)

The use of the decay function assures the numerical stability as well as the accuracy throughout the flow field for a wide range of Reynolds numbers (Refs. 8 and 9).

6.2 GENERAL PROCEDURE WITH A STANDARD GAUSS-SEIDEL POINT ITERATION METHOD

The finite difference equation [Eq. (43)] can be solved in several ways. For simplicity, a standard Gauss-Seidel iteration method is used to obtain the solution. The method updates the field values with the most recent available neighboring point data in the following way:

$$\phi_{i,j}^{n+1} = \frac{C_1 \cdot \phi_{i+1,j}^n + C_2 \cdot \phi_{i-1,j}^{n+1} + C_3 \cdot \phi_{i,j+1}^n + C_4 \cdot \phi_{i,j-1}^{n+1} + d_{i,j}^n}{CU} \quad (45)$$

21

where the superscript n denotes the values at nth iteration, (n+1) denotes the updated value. The coefficients, C_1, C_2,..., C_4 and CU are

$$C_1 = \left(\frac{a_1}{\delta\bar{x}^2}\right)\left(\frac{1}{G_i} - \frac{b_1 \cdot \delta\bar{x}}{2a_1}\right)$$

$$C_2 = \left(\frac{a_1}{\delta\bar{x}^2}\right)\left(\frac{1}{G_i} + \frac{b_1 \cdot \delta\bar{x}}{2a_1}\right)$$

$$C_3 = \left(\frac{a_1}{\delta\bar{r}^2}\right)\left(\frac{1}{G_j} - \frac{b_2 \cdot \delta\bar{r}}{2a_2}\right) \tag{46}$$

$$C_4 = \left(\frac{a_1}{\delta\bar{r}^2}\right)\left(\frac{1}{G_j} + \frac{b_2 \cdot \delta\bar{r}}{2a_2}\right)$$

$$CU = C_1 + C_2 + C_3 + C_4$$

The general flow chart which describes the sequence of the solution procedure is presented in Fig. 4.

7.0 FACTORS AFFECTING THE RATE OF CONVERGENCE OF THE POINT ITERATION METHOD

The advantage of using the Gauss-Seidel point iteration method to solve coupled algebraic equations is well known. The method can be easily programmed and does not require excessive computer storage. However, there are two important factors which affect the rate of convergence, namely, (1) the total number of grid points and (2) the initial flow-field guess. As the total number of grid points is increased to obtain better resolution, the rate of convergence decreases. This is because the information at the boundary points must travel a longer distance to reach the whole flow field in the elliptic type of flow calculations. Since the point iteration method can update only one point value at a time, the larger the number of grid points the slower the convergence rate. On the other hand, the rate of convergence can be greatly improved with a good initial flow-field guess.

22

7.1 INITIAL GUESS FOR DIFFUSER FLOWS

It is well known that a turbulent boundary-layer profile can be represented by the superposition of a logarithmic profile and a wake profile (e.g., Ref. 10). The representation is commonly known as Coles' law of the wake. Coles' concept is generalized in the present approach, with the logarithmic part of the profile replaced by a function related to the fully developed pipe (or channel) flow profile at the diffuser inlet and with the wake portion represented by a cosine function.

The initial velocity field is obtained as a linear combination of the inlet profile and the wake profile, Fig. 5, i.e.,

$$u = u_a + u_b \tag{47}$$

where u_a is related to the inlet velocity profile, u_I, as

$$u_a \left(\frac{r}{SO} \right) = \left(\frac{u_{a,c}}{u_{I,c}} \right) \cdot u_I \tag{48}$$

and the wake component of the profile, u_b is defined as

$$u_b \left(\frac{r}{SO} \right) = u_{b.c} \cdot \frac{1 + \cos \left(\frac{\pi}{SO} \cdot r \right)}{2} \tag{49}$$

The centerline values $u_{a,c}$ and $u_{b,c}$ are the only unknowns in Eqs. (48) and (49). From Eq. (47),

$$u_{a,c} = u_c - u_{b,c} \tag{50}$$

With Eq. (50), Eq. (48) becomes

$$u_a = \frac{u_c - u_{b,c}}{u_{I,c}} \cdot u_I \tag{51}$$

Therefore, the final expression for the velocity profile can be written as

$$u = \frac{(u_c - u_{b,c})}{u_{I,c}} \cdot u_I + u_{b,c} \frac{1 + \cos \left(\frac{\pi}{SO} \cdot r \right)}{2} \tag{52}$$

The unknown $u_{b,c}$ in Eq. (52) can be determined from the conservation of mass. By integrating Eq. (52) across the diffuser, one obtains

$$\int_0^1 u_I \cdot r\,dr = \int_0^{SO(x)} u \cdot r\,dr \tag{53}$$

The right-hand side can be evaluated as

$$\int_0^{SO(x)} u \cdot r\,dr = \int_0^{SO(x)} \frac{(u_c - u_{b,c})}{u_{I,c}} \cdot u_I \cdot r\,dr + \int_0^{SO(x)} u_{b,c} \frac{\left[1 + \cos\left(\frac{\pi}{SO} \cdot r\right)\right]}{2} \cdot r\,dr$$

$$= \frac{(u_c - u_{b,c})}{u_{I,c}} \int_0^{SO(x)} u_I \cdot r\,dr + \frac{u_{b,c}}{2} \left\{\frac{SO^2}{2}\right\}$$

Therefore,

$$\int_0^1 u_I \, r\,dr = \frac{(u_c - u_{b,c})}{u_{I,c}} \int_0^{SO(x)} u_I \cdot r\,dr + \frac{u_{b,c}}{2} \left\{\frac{SO^2}{2}\right\} \tag{54}$$

In terms of the stream function, $\Psi = (\int u\,r\,dr)$, Eq. (54) becomes

$$\Delta\Psi_I = \left(\frac{u_c - u_{b,c}}{u_{I,c}}\right) \cdot (SO)^2 \int_0^1 u_I \cdot \left(\frac{r}{SO}\right) d\left(\frac{r}{SO}\right) + \frac{u_{b,c}}{2}\left\{\frac{SO^2}{2}\right\}$$

$$= \Delta\Psi_I (SO)^2 \left(\frac{u_c - u_{b,c}}{u_{I,c}}\right) + \frac{u_{b,c}}{2}\left\{\frac{SO^2}{2}\right\} \tag{55}$$

where

$$\Delta\Psi = \int_0^1 u_I \, r\,dr$$

Solving for $u_{b,c}$, one obtains

$$u_{b,c} = \frac{\Delta\Psi \left[1 - (SO)^2 \frac{u_c}{u_{I,c}}\right]}{\frac{SO^2}{4} - SO^2 \cdot \Delta\Psi \frac{1}{u_{I,c}}} \tag{56}$$

When the wake component vanishes, i.e., $u_{b,c} = 0$, Eq. (56) becomes

$$1 - (SO)^2 \frac{u_c}{u_{I,c}} = 0 \tag{57}$$

or

$$u_c = \frac{u_{I,c}}{(SO)^2} \tag{58}$$

In general, the wake component $(u_{b,c})$ is nonzero and the centerline velocity (u_c) is greater than that given by Eq. (58). In order to increase u_c value from Eq. (58), an effective area concept is introduced as

$$u_c = \frac{u_{I,c}}{(SO_{eff})^2} \tag{59}$$

The simplest form of SO_{eff} is

$$SO(x)_{eff} = [SO(x) - 1] \times \lambda + 1.0 \tag{60}$$

where $SO(x)_{eff}$ is shown in Fig. 6

The unknown constant λ $(0 \leq \lambda \leq 1.0)$ depends upon the diffuser divergence angle. In general, the value of λ decreases from unity as the divergence angle increases. No formula has been derived to determine the exact value of λ. Therefore, its specification requires some experience about the diffuser flow solution. For an inexperienced user, in general, $\lambda = 0.5$ is a good initial guess.

The complete initial flow-field distribution of the velocity, the vorticity, and the stream function (u, Ω, Ψ) can be derived from Eqs. (56) and (47) as

$$u\left(\frac{r}{SO}\right) = u_I(r) \cdot \frac{u_c - u_{b,c}}{u_{I,c}} + u_{b,c} \frac{1 + \cos\left(\frac{\pi}{SO} r\right)}{2} \tag{61}$$

$$\Omega\left(\frac{r}{SO}\right) = \Omega_I(r) \cdot \frac{u_c - u_{b,c}}{u_{I,c}} + \frac{u_{b,c}}{2}\left(\frac{\pi}{SO}\right) \cdot \sin\left(\frac{\pi}{SO} \cdot r\right) \tag{62}$$

$$\Psi\left(\frac{\pi}{SO}\right) = \Psi_I(r) \cdot \frac{(u_c - u_{b,c})(SO)^2}{u_{I,c}} + \frac{u_{b,c}}{2}\left\{\frac{r^2}{2} + \frac{SO}{\pi} \cdot \left[r \cdot \sin\left(\frac{\pi}{SO} \cdot r\right)\right.\right.$$
$$\left.\left. - \sin\left(\frac{\pi}{SO} \cdot r\right)\right]\right\} \tag{63}$$

25

$$\nu_t \left(\frac{r}{SO}\right) = \nu_{t,I} \; (r) \cdot \frac{(u_c - u_{b,c})}{u_{I,c}} + 0.1 * \frac{u_{b,c}}{2} \cdot \left[\pi \cdot \sin \left(\frac{\pi}{SO} \cdot r\right)\right] \qquad (64)$$

for any axial location, x.

7.2 MULTIPLE GRID GAUSS-SEIDEL ITERATION METHOD

The Gauss-Seidel iteration method is a point iteration method which updates one point at a time with the most recently available values at the neighboring points. It can be easily seen that the rate at which the information from a boundary is propagated to the rest of the flow field depends upon the total number of the grid points in the flow field. When the flow-field pattern is fairly complicated and it is necessary to use a large number of grid points to improve the accuracy of the final solution, the rate of convergence becomes slow with the point Gauss-Seidel iteration method. A simple and efficient multiple grid method has been developed to speed the rate of convergence.

A series of grid systems can be constructed for a rectangular domain, Fig. 7, with grid spacing ratio equal to $(1/2)^N$.

The general multiple grid Gauss-Seidel iteration scheme can be written as

Do $\underline{100}$ J = JL , JR , L

Do $\underline{100}$ I = IL , IR , L

$$\phi_{i,j}^{n+1} = (C_1 \; \phi_{i+L,j}^{n} + C_2 \; \phi_{i-L,j}^{n+1} + C_3 \; \phi_{i,j+L}^{n} - C_4 \; \phi_{i,j-L}^{n+1} \qquad (65)$$

$$+ D^n) \Big/ (C_1 + C_2 + C_3 + C_4)$$

-----

100 Continue

26

With L equal to unity, one recovers the conventional single grid system Gauss-Seidel method. For a dual system, L is set equal to two for the first N iterations to obtain a solution for the coarse grid system. Before continuing to a finer grid system (with L = 1), it is necessary to obtain the midpoint value with a linear interpolation scheme. The flow chart for the process is shown in Fig. 8. Since the coarse grid system has only one-fourth of the total grid points of the finer system, the rate of convergence is a factor of four faster. Another advantage is that the fast convergent solution obtained in the coarse grid system is used to obtain the initial guess for the finer grid system through an interpolation routine. In the present solution procedure, a dual grid system, i.e., from a 17 by 31 coarse system to a 33 by 61 fine grid system is adequate. The operation is done automatically in the computer program.

8.0 RESULTS AND DISCUSSION

The numerical formulation and the turbulence model presented in the previous sections are applied to the computation of several conical diffuser flows.

Although much experimental data on the performance of subsonic diffusers are available, few of these data are suitable for verification of the numerical analysis. The major emphasis in most experimental investigations has been placed on overall performance, i.e., pressure recovery, and only rarely were the mean velocity profiles at the inlet section and in the divergent section measured. Even more rare are experiments in which the turbulence properties in the flow field were measured. Recently, however, experimental data on both the mean velocity and turbulence properties in an 8-deg conical diffuser were obtained by Okwuobi and Azad (Ref. 4); the inlet flow was a fully developed pipe flow. These data provide a good test case for comparison with the numerical analysis because the fully developed entry conditions are well

27

established and can be predicted with confidence. In addition to the correlations of the Okwuobi and Azad experiment, comparison of the numerical results with other experiments (in which the inlet conditions are less well-defined) are described in this section.

8.1 NUMERICAL SOLUTIONS OF 8-DEG CONICAL DIFFUSER WITH A FULLY DEVELOPED INLET PROFILE

The geometry of the 8-deg conical diffuser is shown in Fig. 9. The area ratio is 4:1. The computed velocity field at several axial stations is also shown in Fig. 9. It can be seen that the velocity profile changes from that of a fully developed inlet pipe flow into a wake profile in the diverging section. The law of the wall region also diminishes and the wake portion of the profile becomes dominant at the exit section of the diffuser. The comparison between the computed and the measured velocity profiles at two stations is shown in Fig. 10. The agreement between the experiment and theory is excellent. In order to check the sensitivity of the computed flow field to the present turbulence model, a small perturbation on the c_μ formula from

$$c_\mu = c_{\mu o} - \Delta c_\mu$$

to

$$c_\mu = c_{\mu o} - 1.4 \, \Delta c_\mu \tag{66}$$

was used. The modification has no effect on the fully developed inlet velocity profile because the flow is parallel so that the radial velocity component, v, vanishes. The velocity profile at the downstream station ($x/D_I = 5.95$) is only slightly changed by the c_μ perturbation as shown in Fig. 10.

The velocity profile near the wall is shown in Fig. 11. The linearity of the velocity profile in the sublayer region is clearly evident and the agreement with the experimental data is excellent.

The decay of the centerline velocity is shown in Fig. 12 for two c_μ models. The $c_\mu = c_{\mu o}$ model gives a faster velocity decay as expected. On the other hand, results obtained from the new c_μ expression agree very well with the experimental data.

The total shear stress distribution is given in Fig. 13. The computed results agree well with the measured total shear stress at $x/D_I =$ 1.19 in the diverging section. At the downstream station ($x/D_I =$ 5.95), although the shape of the total shear stress profile is qualitatively correct, the maximum predicted value is about 15 percent higher than the measured value. The measured turbulent kinetic energy distribution, Fig. 14, is also lower than the prediction at the downstream station, especially near the wall. In this region, the turbulent fluctuation velocities are of the same order of magnitude as the local velocity (u). In this situation, the hot-wire probe measurement is questionable. Usually, the x-probe yields a lower measurement of the turbulent intensity because of the higher instantaneous flow angularity and negative velocity, hence an underestimated shear stress and TKE. The agreement between calculated and measured TKE near the diffuser inlet is quite good. The calculated turbulent kinetic energy distribution near the wall, shown in Fig. 15, is lower at the downstream station than at the inlet. This is caused by the lower TKE production associated with the downstream velocity profile. The ratio between the shear stress $\overline{u'v'}$ and the TKE is shown in Fig. 16. At the inlet, the ratio quickly rises to a maximum value of 0.3 and drops gradually to zero at the centerline. Experimental data for fully developed pipe flow by Laufer (Ref. 11) are also included in Fig. 16 for comparison. At the downstream station, the profile is skewed toward the centerline and the maximum value of the ratio also increases slightly.

In Fig. 17, the distribution of the eddy viscosity coefficient, c_μ, is shown for several axial stations. At the inlet, the c_μ distribution is identical to that of the previous model since the Δc_μ

29

term is zero. The c_μ distribution drops immediately in the diverging section. The level of c_μ then increases slowly with increasing distance in the diverging section. It is important to note that the average value of c_μ in the diverging section is always lower than the inlet c_μ level.

The wall pressure coefficient, C_p, is presented in Fig. 18. The computed pressure coefficients agree well with measured values except that they are somewhat overpredicted in the downstream stations. Part of this difference could be attributed to the effect of the computational grid size. Another factor is that the numerical computation is carried out for a diffuser with a tail pipe while the experimental configuration did not have a tail pipe. It has been shown, Refs. 12 and 13, that the tail pipe increases the pressure recovery somewhat. Therefore, the higher predicted pressure recovery is consistent with experimental evidence.

8.2 NUMERICAL SOLUTION OF 8-DEG CONICAL DIFFUSER WITH A BOUNDARY-LAYER INLET PROFILE

Computations of an 8-deg conical diffuser flow field were made with two inlet boundary-layer thicknesses. The velocity distribution for the thin boundary-layer case, $\delta_I = 0.05\ D_I$, is shown in Fig. 19. The difference between the velocity profile with a boundary layer and the fully developed one is the existence of a potential core. It can be seen from Fig. 19 that the potential core remains throughout the diffuser section. The wall pressure coefficient, C_p, is shown in Fig. 20. Comparison with the experimental pressure recovery is good.

The velocity distributions for the thicker boundary-layer case, $(\delta_I = 0.2\ D_I)$ are shown in Fig. 21. The potential core region is smaller than in the thin boundary-layer case, otherwise, the development of boundary-layer profiles is about the same. The total shear stress

distribution is shown in Fig. 22. Upstream of the inlet, the total shear stress is highest and constant near the wall, i.e., $\tau_{tot} = \tau_w$. In the diffuser section, the maximum total shear stress location moves away from the wall and the maximum value increases. The shear stress along the wall decreases in the diverging section. The turbulent kinetic energy distribution is shown in Fig. 23. The free-stream turbulence level was set equal to one percent which remains approximately constant in the potential core region. Just as was observed for the shear stress, the location of the maximum TKE moves away from the wall in the diverging section. The eddy viscosity distribution, normalized by the local centerline velocity and the local boundary-layer thickness, is shown in Fig. 24. Notice that, as x increases, the maximum eddy viscosity increases greatly from the boundary-layer value of order 0.001 near the entrance to almost the turbulent mixing layer value of order 0.01 at the downstream station. The length scale derived from the turbulent kinetic energy dissipation is shown in Fig. 25. The maximum normalized length scale in the boundary layer increases from 0.65 to about 1.4 between the inlet station and the downstream station. Finally, the wall pressure coefficient, C_p, is presented in Fig. 26. The exit value of 0.77 is slightly lower than the previous case with a thinner inlet boundary layer (C_p = 0.8). This is consistent with experimental evidence that C_p decreases with increasing inlet boundary-layer thickness and that C_p increases again when the inlet condition is fully-developed (Refs. 13 and 14). The effect of the inlet boundary-layer thickness on the pressure recovery coefficient for an 8-deg conical diffuser is shown in Fig. 27. Although the trend is well predicted, the predicted C_p level is higher than the data of Ref. 13.

8.3 NUMERICAL SOLUTION OF 16-DEG CONICAL DIFFUSER WITH A BOUNDARY-LAYER INLET PROFILE

The computed velocity distribution for a 16-deg conical diffuser with a thin inlet boundary layer (δ_I = 0.05 D_I) is shown in Fig. 28.

31

The velocity at the exit station (x/D_I = 3.58) is negative near the wall indicating that the flow is separated. This is in agreement with the experimental evidence observed by McDonald and Fox, Ref. 15, and Senoo and Nishi, Ref. (12), who found the 16-deg conical diffuser with an area ratio of four lies within the separated flow regime of the diffuser performance map. The pressure coefficient C_p is shown in Fig. 29. The agreement with the experimental data (Ref. 12) is qualitatively good. The experimentally observed separation point detected by tufts lies somewhat ahead of the predicted point of separation. This could be caused by the coarse grid size (Δx) used in the computation. However, the use of tufts only provides a crude estimate of the point of separation. Thus, the agreement is probably as good as one could expect.

8.4 NUMERICAL SOLUTION OF 13-DEG CONICAL DIFFUSER WITH A BOUNDARY-LAYER INLET CONDITION

The measured and calculated velocity distribution for a 13-deg conical diffuser is shown in Fig. 30. The agreement with the data, Ref. 16, is qualitatively good at x/D_I = 3.2. The experimental data, obtained with an x-probe hot wire, shows a larger tail region near the edge of the boundary layer. Near the wall, the hot-wire measurement is slightly higher than the calculated velocity values because of high local relative turbulent intensity. At a far downstream station, x/D_I = 5.9, the flow separation is clearly indicated in the calculated velocity profile. Under the separated flow condition, the conventional hot-wire probe is not capable of distinguishing the positive and negative velocities. As a result, the hot-wire measurement is always positive in the separated flow region. The pressure coefficient C_p is shown in Fig. 31. The agreement between the data and the computed value is good. The predicted value of C_p is slightly higher than the data at the exit. The point of separation is also included in Fig. 31. The present predicted point of separation lies among the separation points predicted with various assumptions in the boundary-layer theory (Ref. 16). No experi-

mental evidence of the point of separation was obtained. Furthermore, no comparisons were made between the computed turbulence flow field and the data because of the apparent misalignment problem of the hot-wire x-probe used in the experiment as discussed in Boldman's report (Ref. 16).

9.0 CONCLUDING REMARKS

The important results of this analytical and numerical study of turbulent flows in conical subsonic diffusers are:

1. A c_μ formula for axisymmetrical flows has been developed for the low Reynolds number, two-equation k-ε turbulence model which unifies the computation of 2D planar and axisymmetrical flows.

2. An initial guess procedure and a multiple grid Gauss-Seidel iteration method have been developed to increase the rate of convergence.

3. Numerical computations of several separated and nonseparated conical diffuser flow fields, with nonuniform inlet condition varying from a fully developed pipe flow profile to a thin boundary-layer profile, are in good agreement with available experimental data.

REFERENCES

1. Chien, J. C. "Numerical Analysis of Turbulent Separated Subsonic Diffuser Flows." AEDC-TR-76-159 (ADA036005), February 1977.

2. Launder, B. E., Rodi, W., and Spalding, D. B. "Prediction of Free Shear Flows, a Comparison of the Performance of Six Turbulence Models." NASA SP-321, 1972.

3. Rodi, W. "A Note on the Empirical Constant in the Kolmogorov-Prandtl Eddy-Viscosity Expression." Journal of Fluids Engineering, Transactions of the ASME, Sept. 1975. pp. 386-389.

4. Okwuobi, P. A. C. and Azad, R. S. "Turbulence in a Conical Diffuser with Fully Developed Flow at Entry." Journal of Fluid Mechanics, Vol. 57, Part 3, 1973, pp. 603-622.

5. Townsend, A. A. The Structure of Turbulent Shear Flow. Cambridge Press, 1956, p. 189.

6. Schlichting, H. Boundary Layer Theory. Fourth Edition, McGraw Hill Book Co., 1960.

7. Abramovich, G. N. The Theory of Turbulent Jets. The MIT Press. 1963, p. 81.

8. Chien, J. C. "A General Finite-Difference Formulation with Application to Navier-Stokes Equation." Journal of Computational Physics, Vol. 20, No. 3, March 1976, pp. 268-278.

9. Chien, J. C. "A General Finite Difference Formulation with Application to Navier-Stokes Equations." Computers and Fluids, Vol. 5, No. 1, March 1977, pp. 15-31.

10. Hinze, J. O. Turbulence. McGraw-Hill Book Company, New York, 1959, p. 507.

11. Laufer, John. "The Sturcture of Turbulence in Fully Developed Pipe Flow." NACA Report 1174, 1954 or Hinze, J. O. Turbulence. McGraw-Hill Book Company, 1959, p. 524.

12. Senoo, Y, and Nishi, M. "Improvement of the Performance of Conical Diffusers by Vortex Generators." Journal of Fluids Engineering, Transactions of the ASME, March 1974, pp. 4-10.

13. Cockrell, D. J. and Markland, E. "A Review of Incompressible Diffuser Flow." Aircraft Engineering, 35, 1963, pp. 286-292.

14. Bradshaw, P. "Performance of a Diffuser with Fully-Developed Pipe Flow at Entry." Journal of Royal Aeronautical Society, Vol. 67, 1963, p. 733.

15. McDonald, A. T. and Fox, R. W. "An Experimental Investigation of Incompressible Flow in Conical Diffusers." International Journal of Mechanical Sciences, Vol. 8, Pergamon Press Ltd., 1966, pp. 125-139.

16. Boldman, D. R. and Newmann, H. E. "Experimental and Analytical Study of a Conically Diffused Flow with a Nearly Separated Boundary Layer." NASA TN D-7486, November 1973.
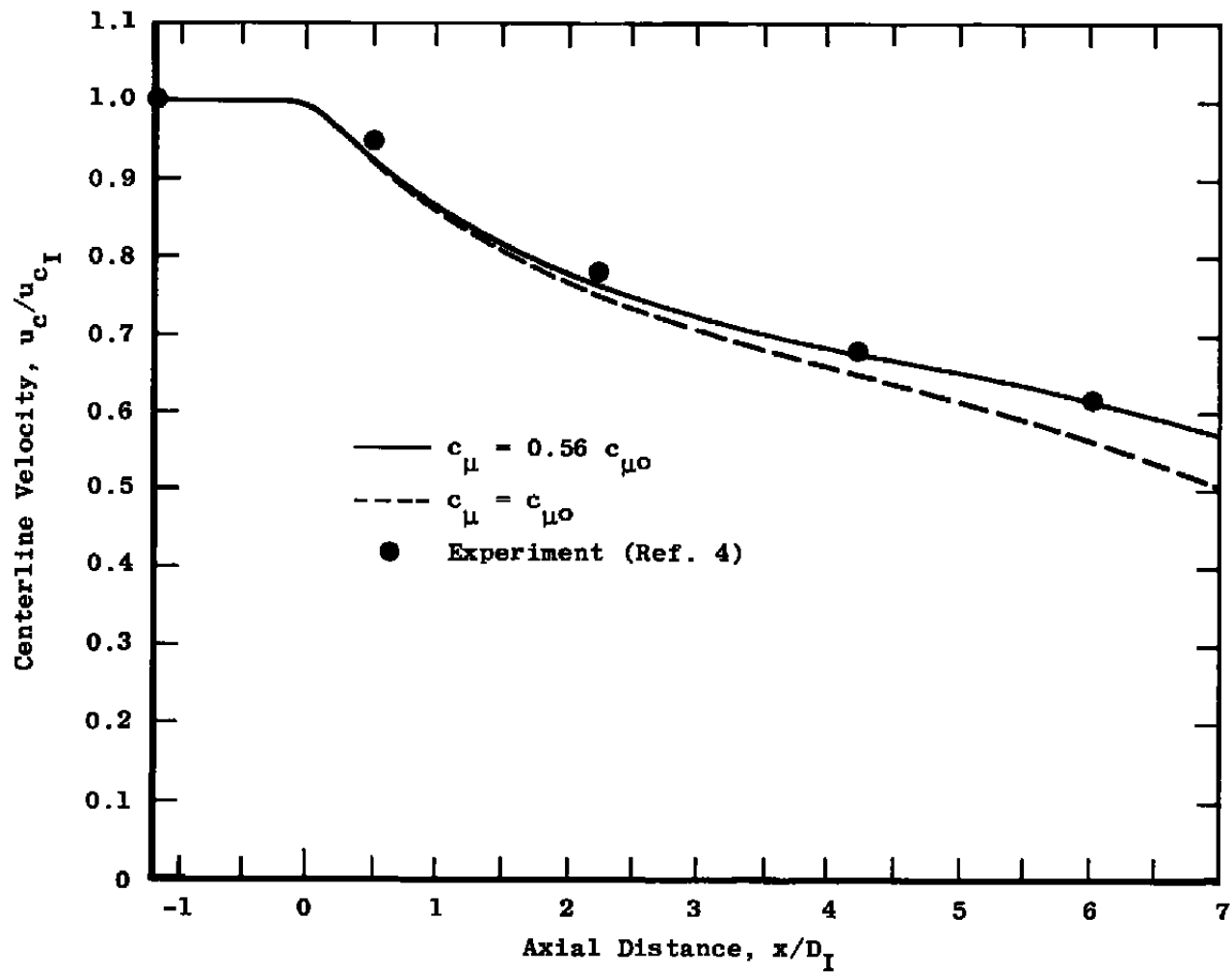
Figure 1. Centerline velocity distribution in 8-deg conical diffuser.
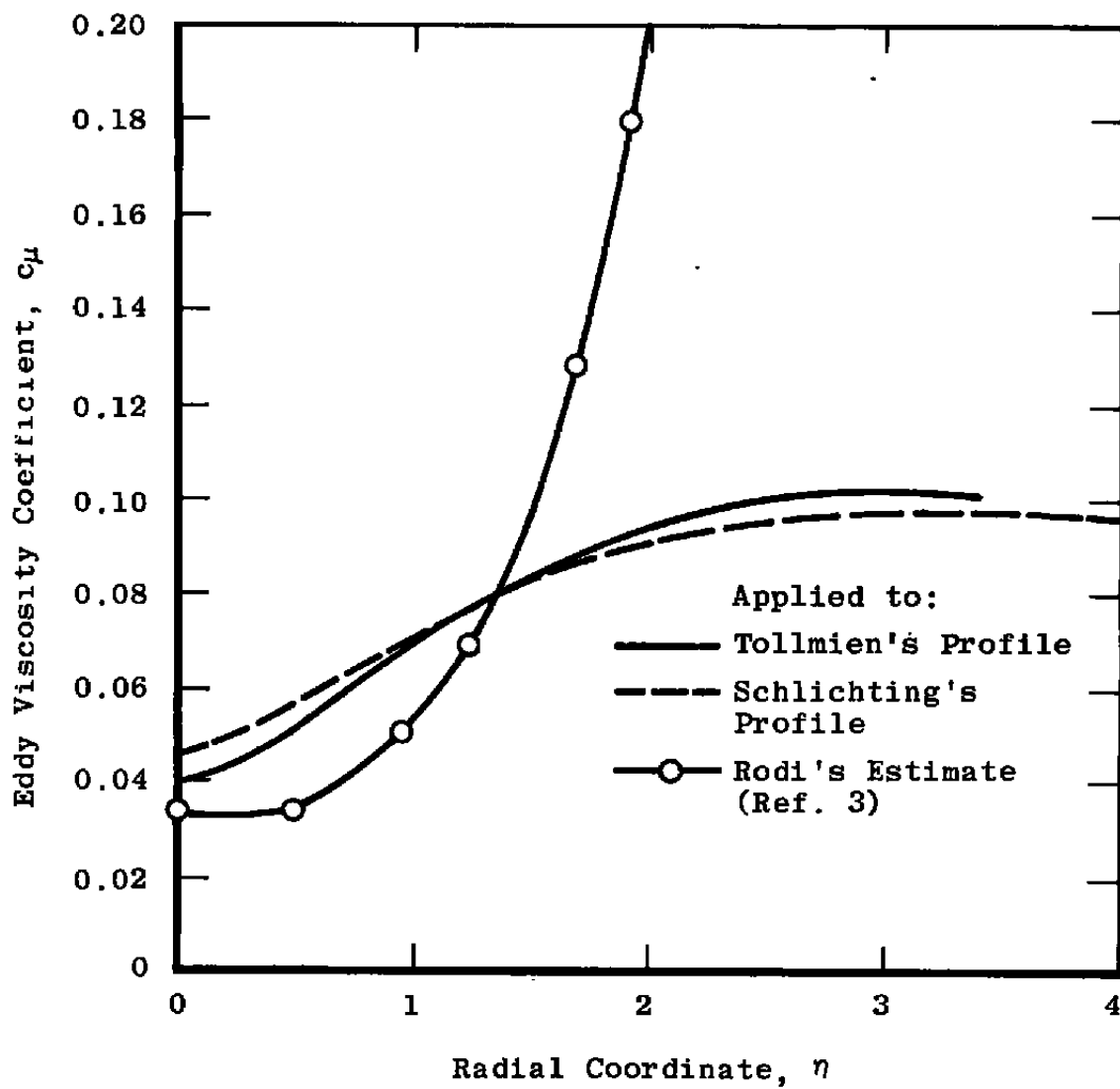
Figure 2. Distribution of the eddy viscosity coefficient, c_μ, for a round jet.
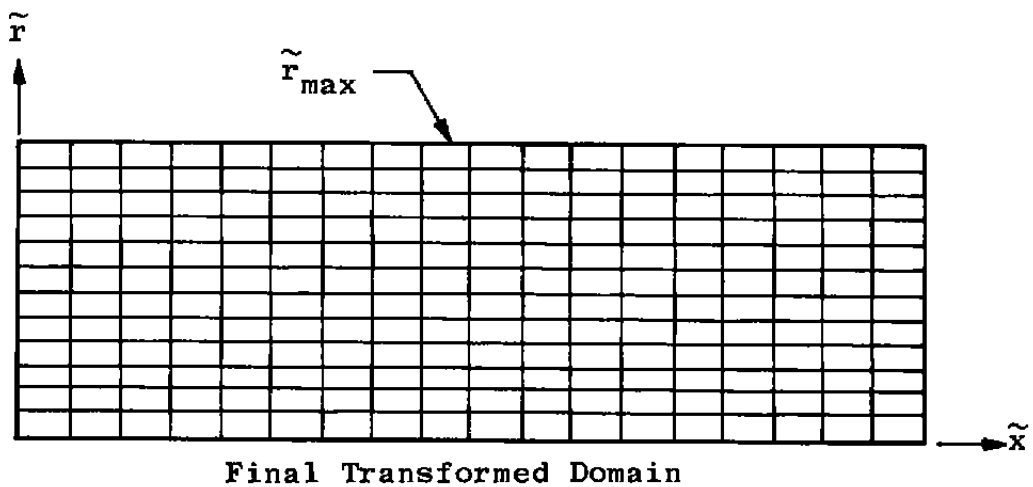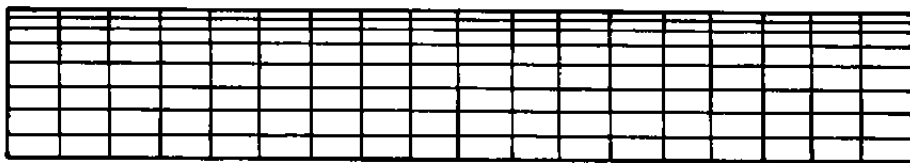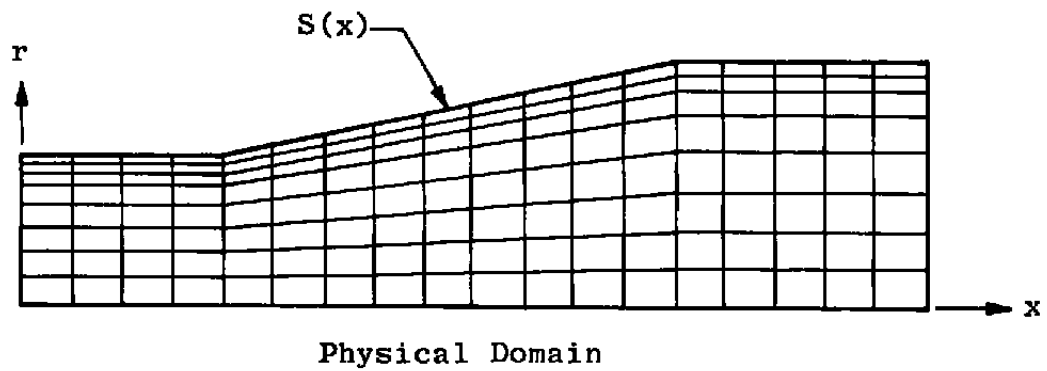
Figure 3. A complete tranformation for a diffuser.
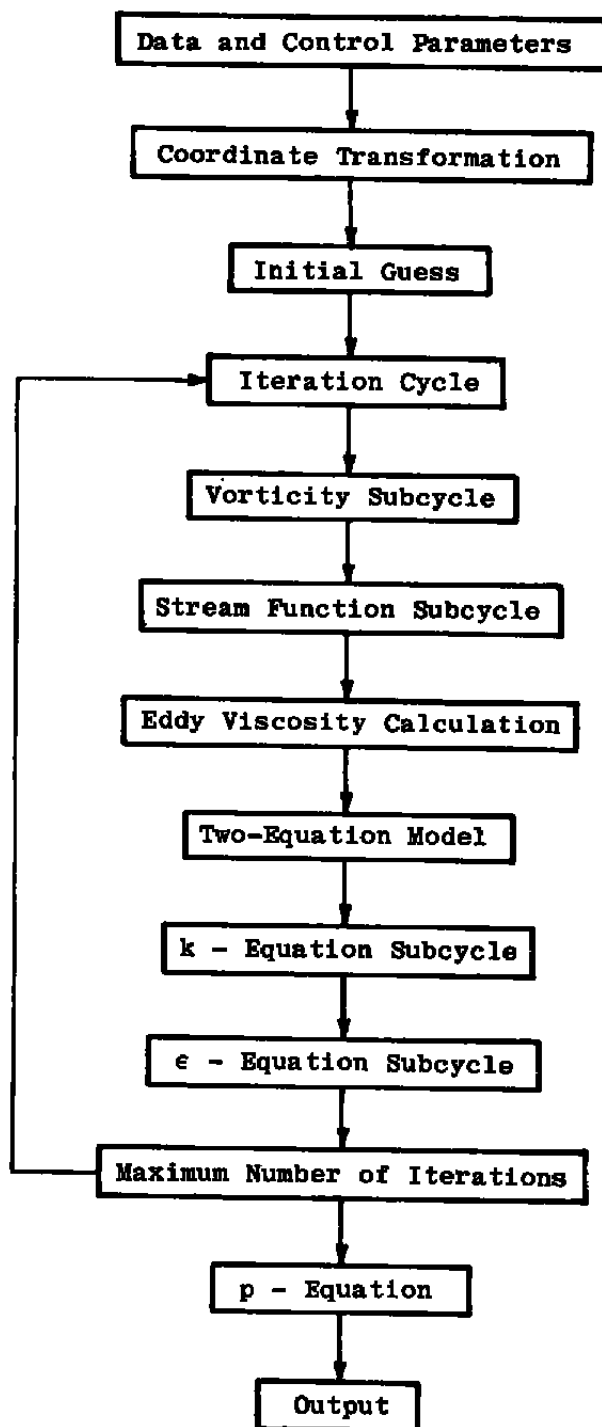
Figure 4. Flow chart of the solution procedures.
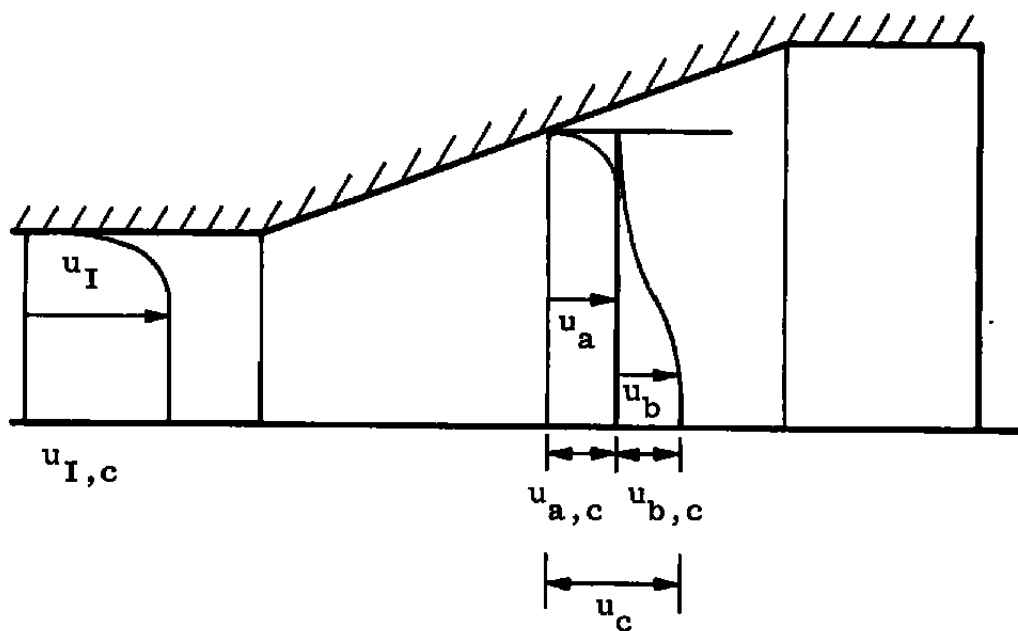
Figure 5. Construction of initial velocity distribution.
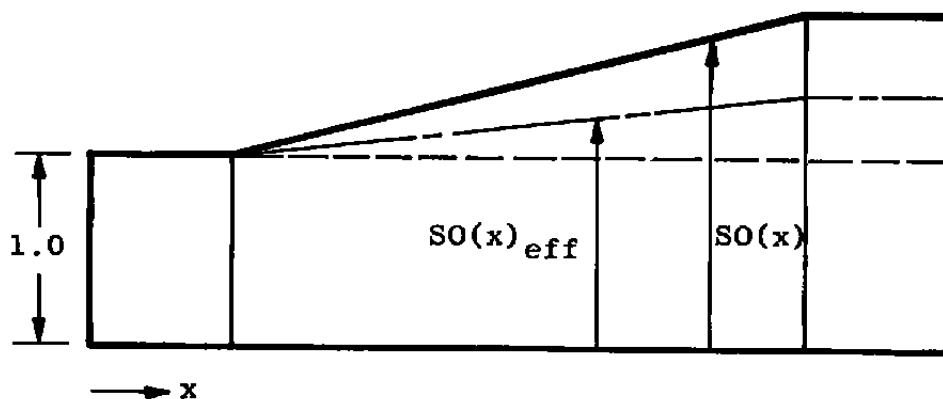
Figure 6. Effective area concept for initial centerline
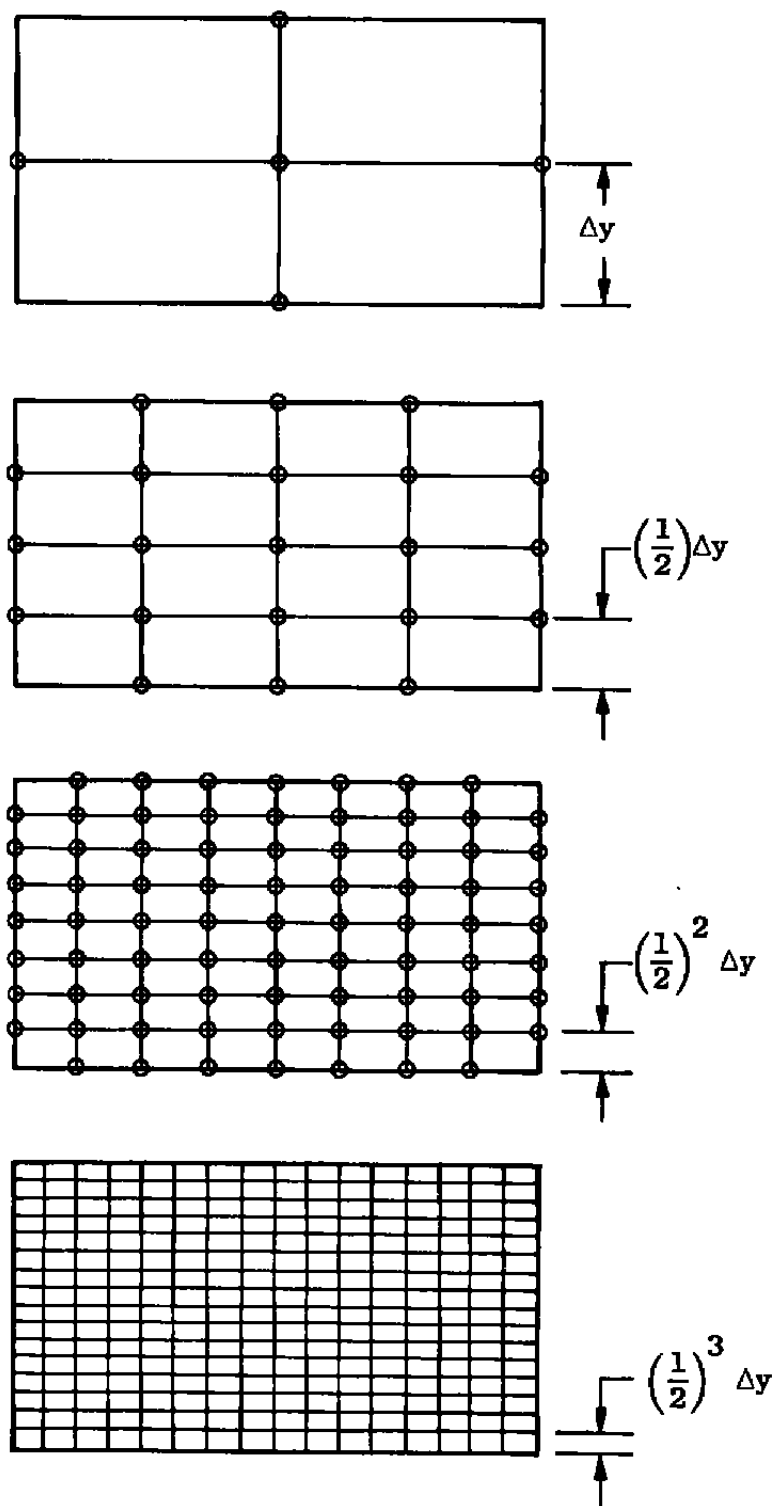velocity distribution.

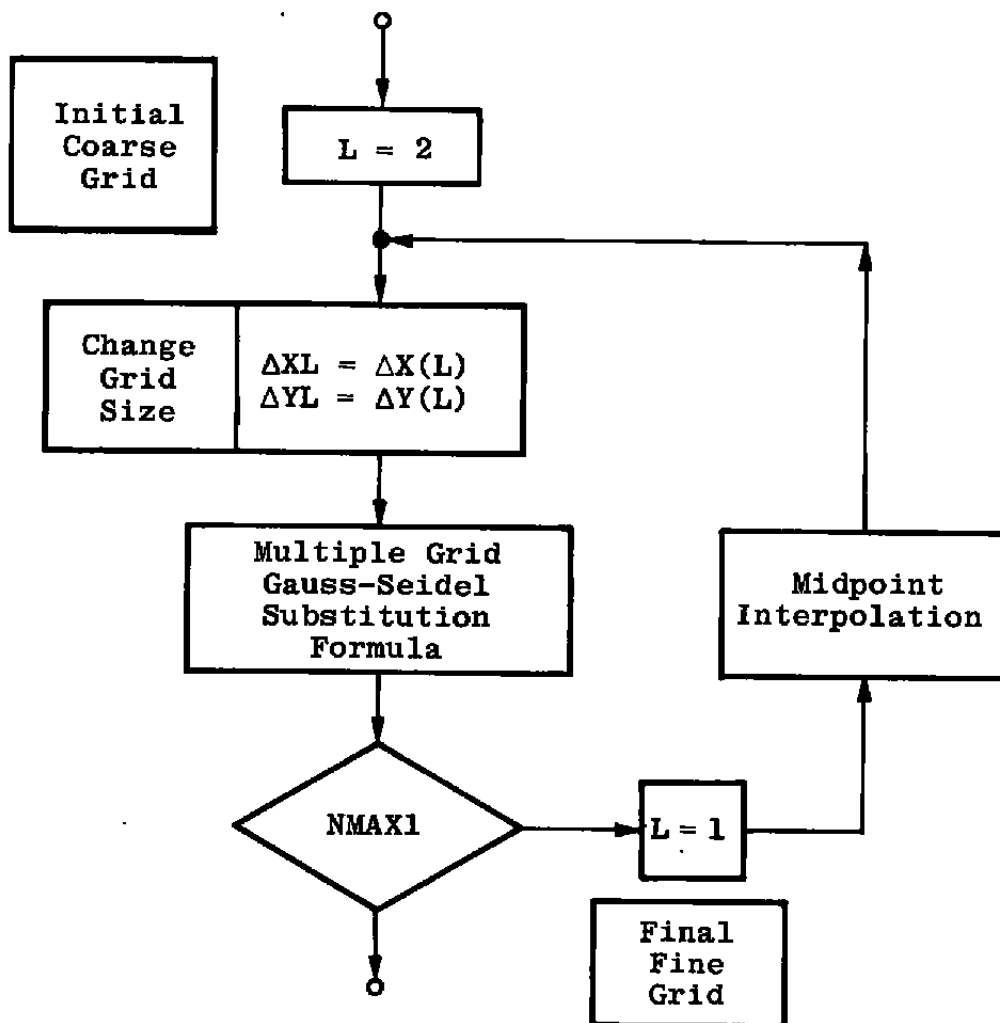Figure 7. A multiple grid system for rectangular computational domain.

Figure 8. A dual grid Gauss-Seidel iteration scheme.
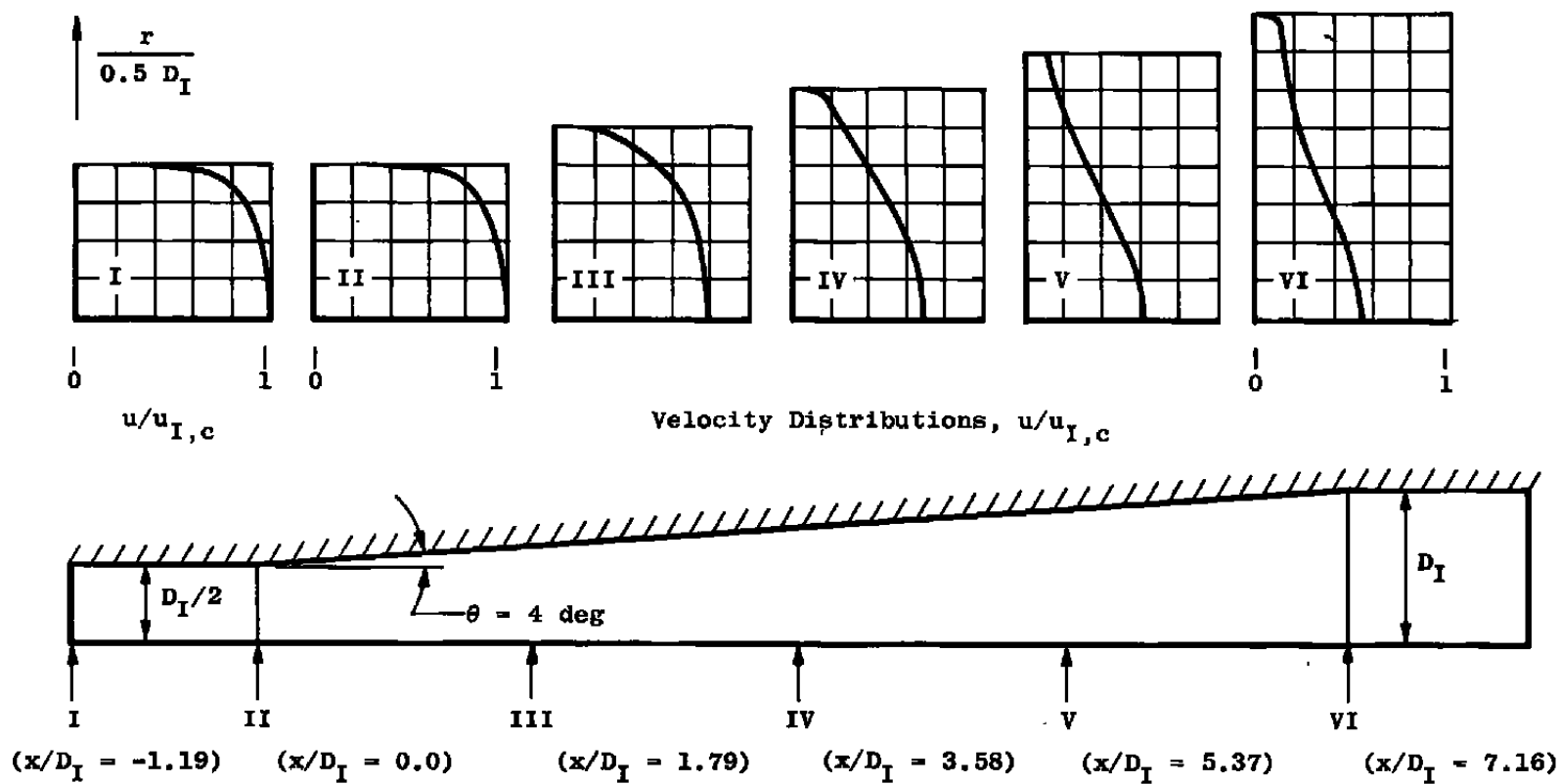
Figure 9. Development of velocity profiles in 8-deg conical diffuser.
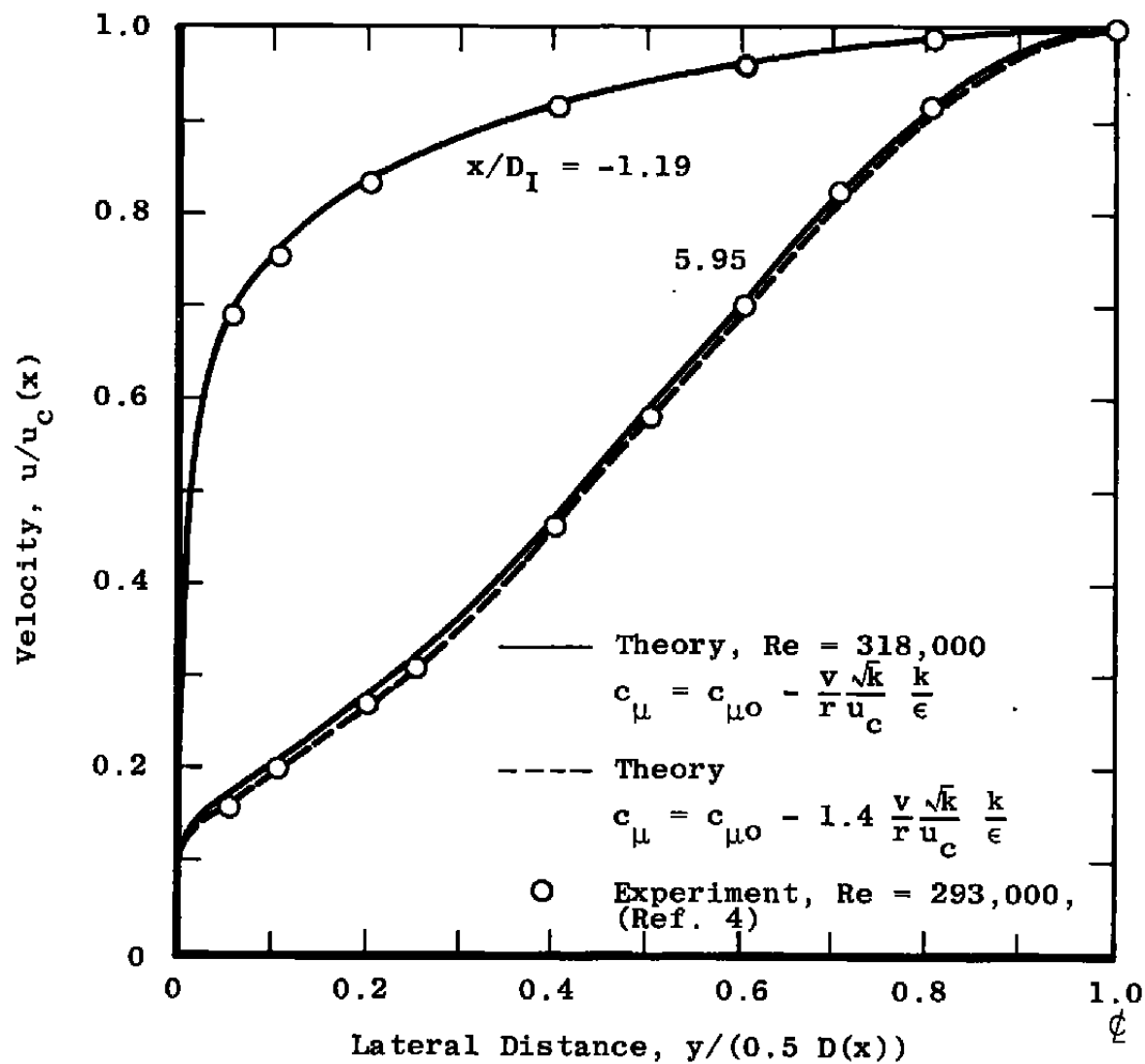
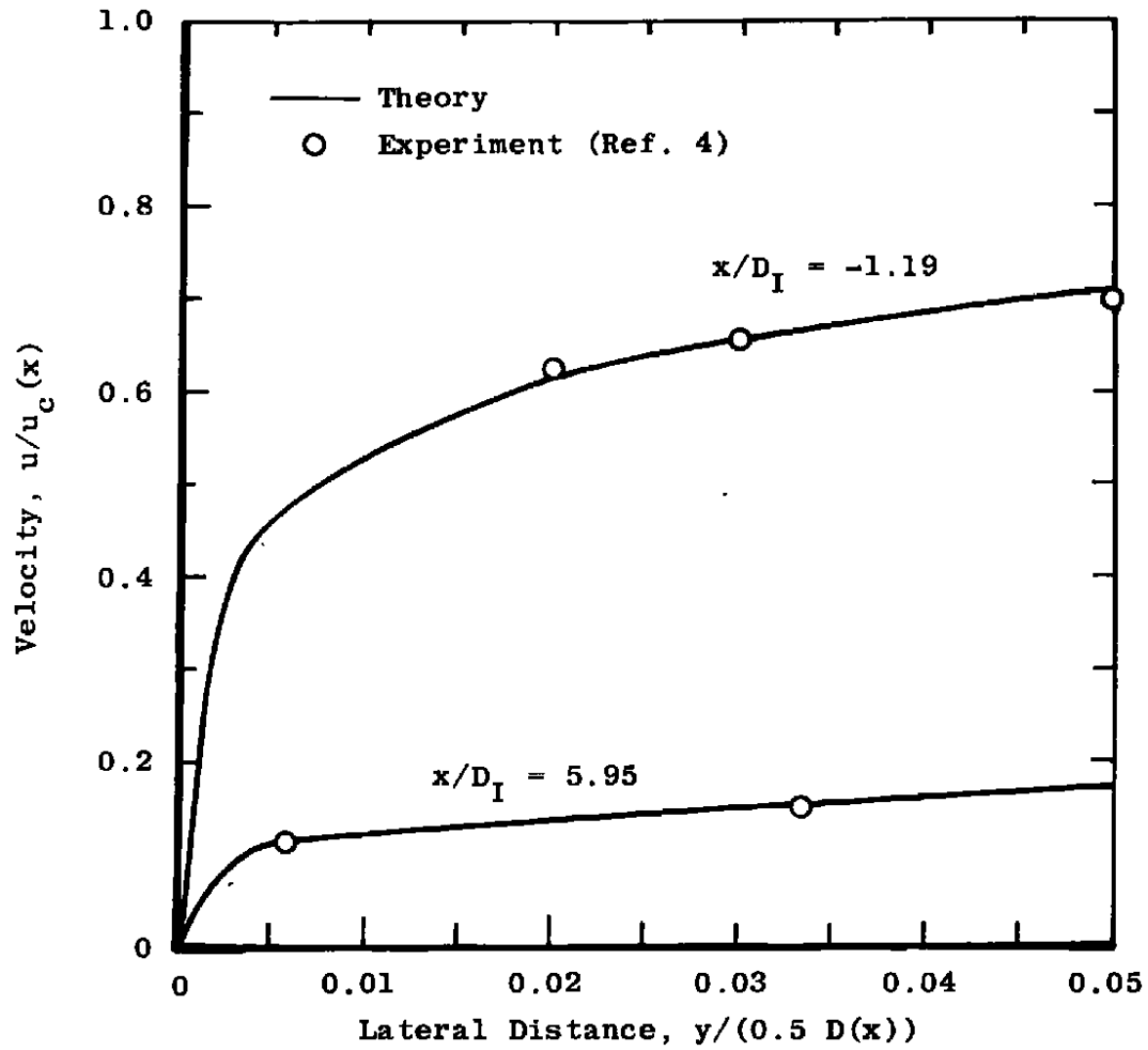Figure 10. Velocity distributions in 8-deg conical diffuser.

Figure 11. Velocity distributions near the wall in 8-deg conical diffuser.
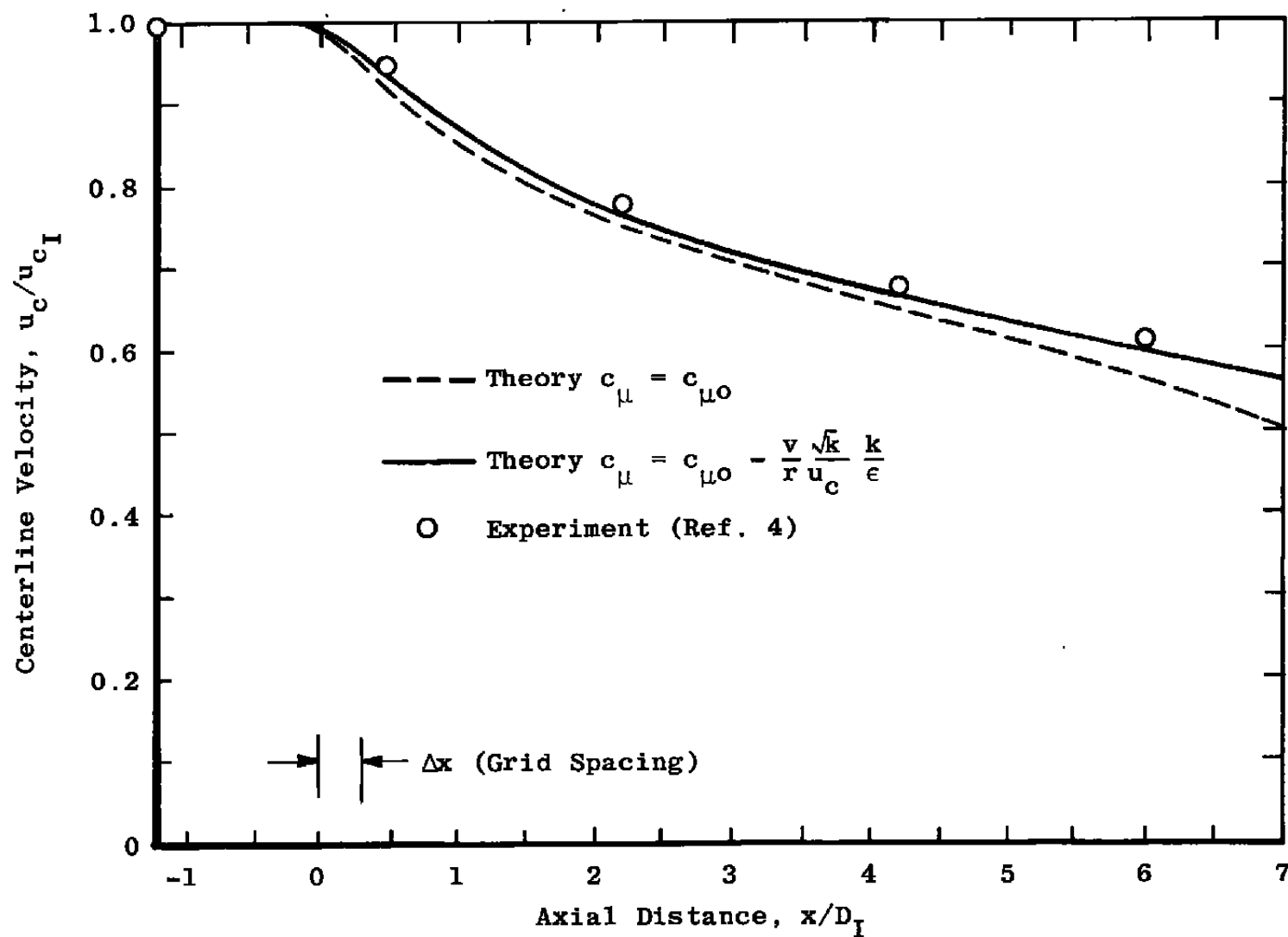
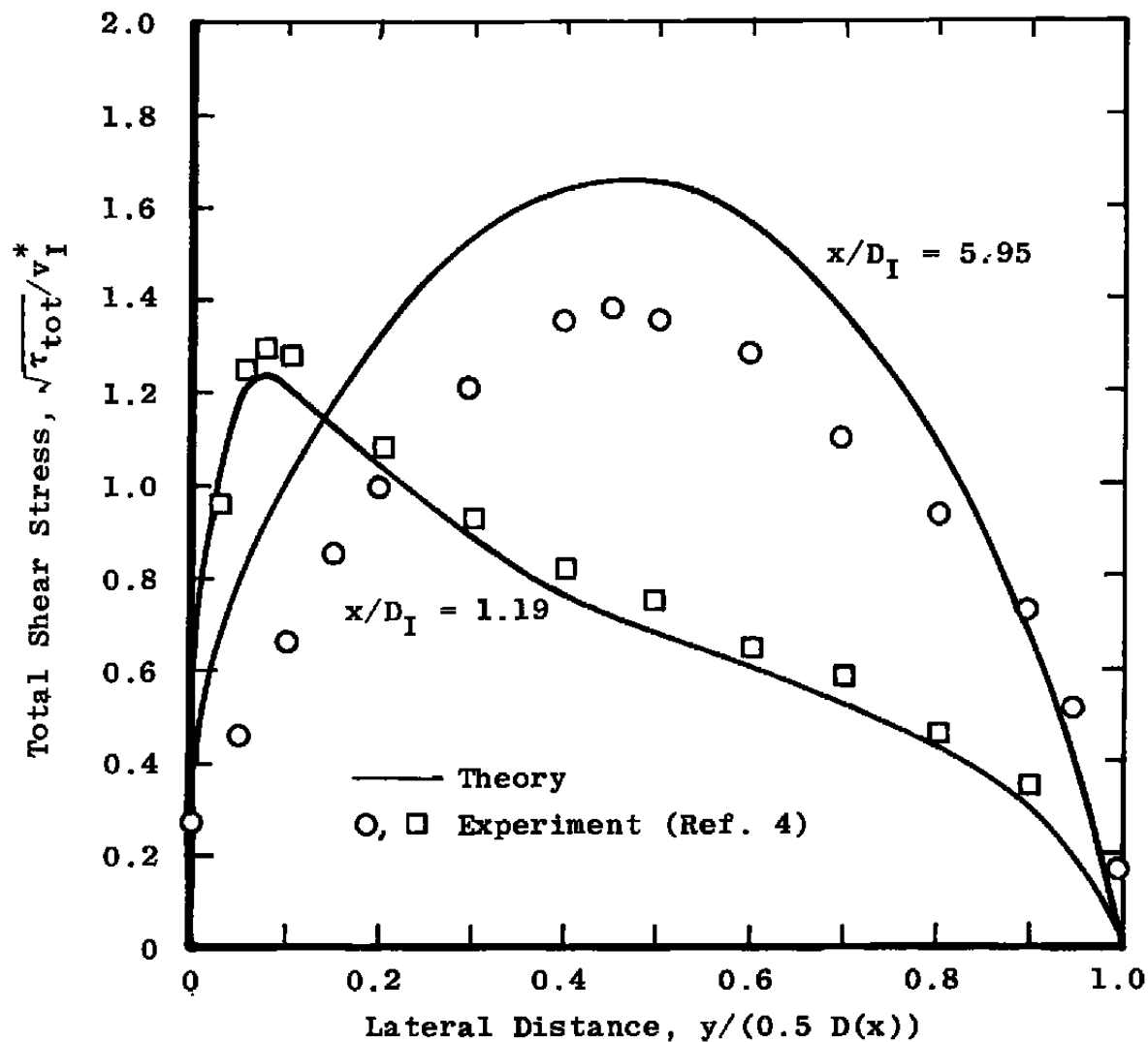Figure 12. Centerline velocity distribution in 8-deg conical diffuser.

Figure 13. Total shear stress distributions in 8-deg conical diffuser.
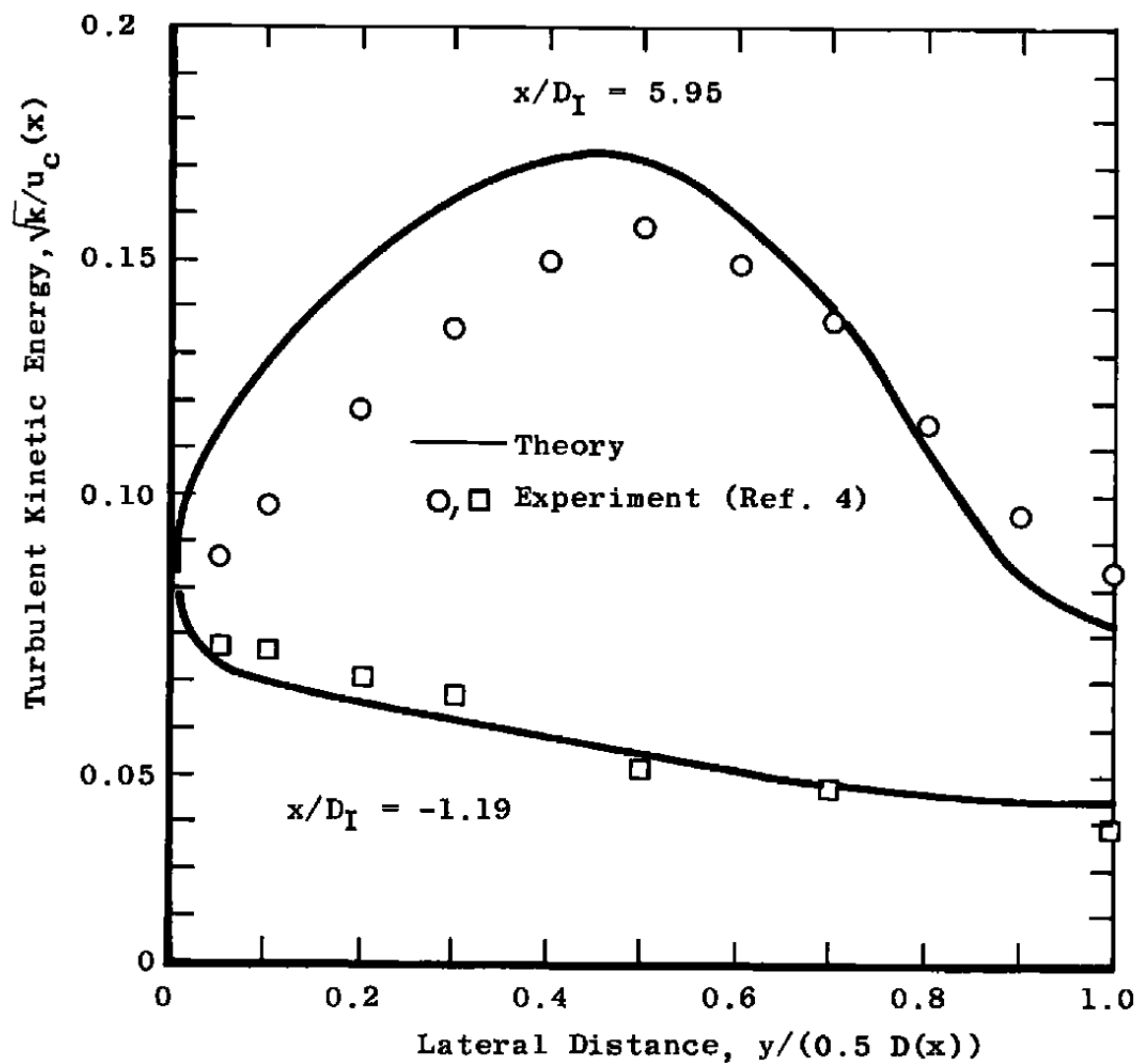
Figure 14. Turbulent kinetic energy distributions in 8-deg conical diffuser.
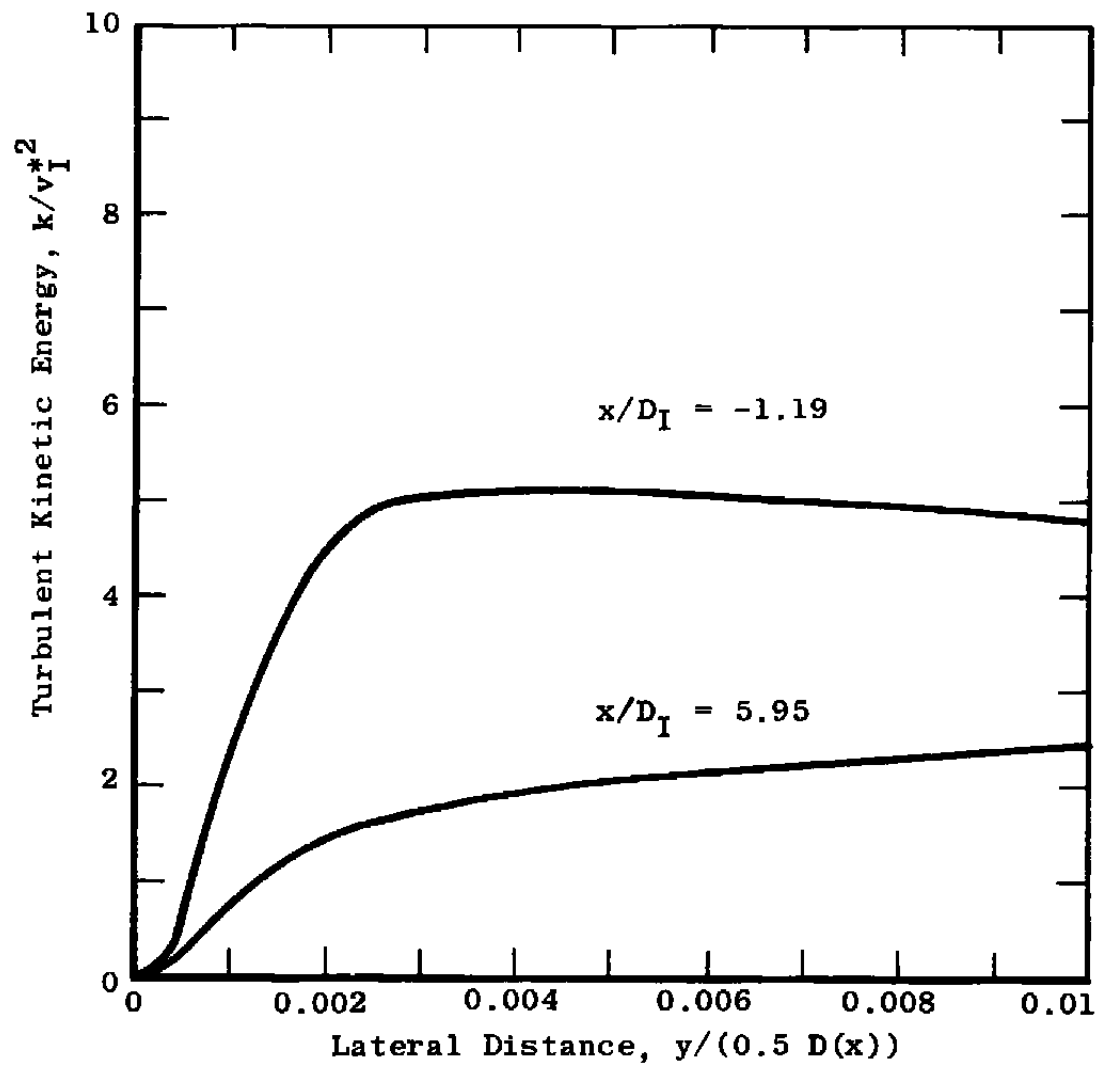
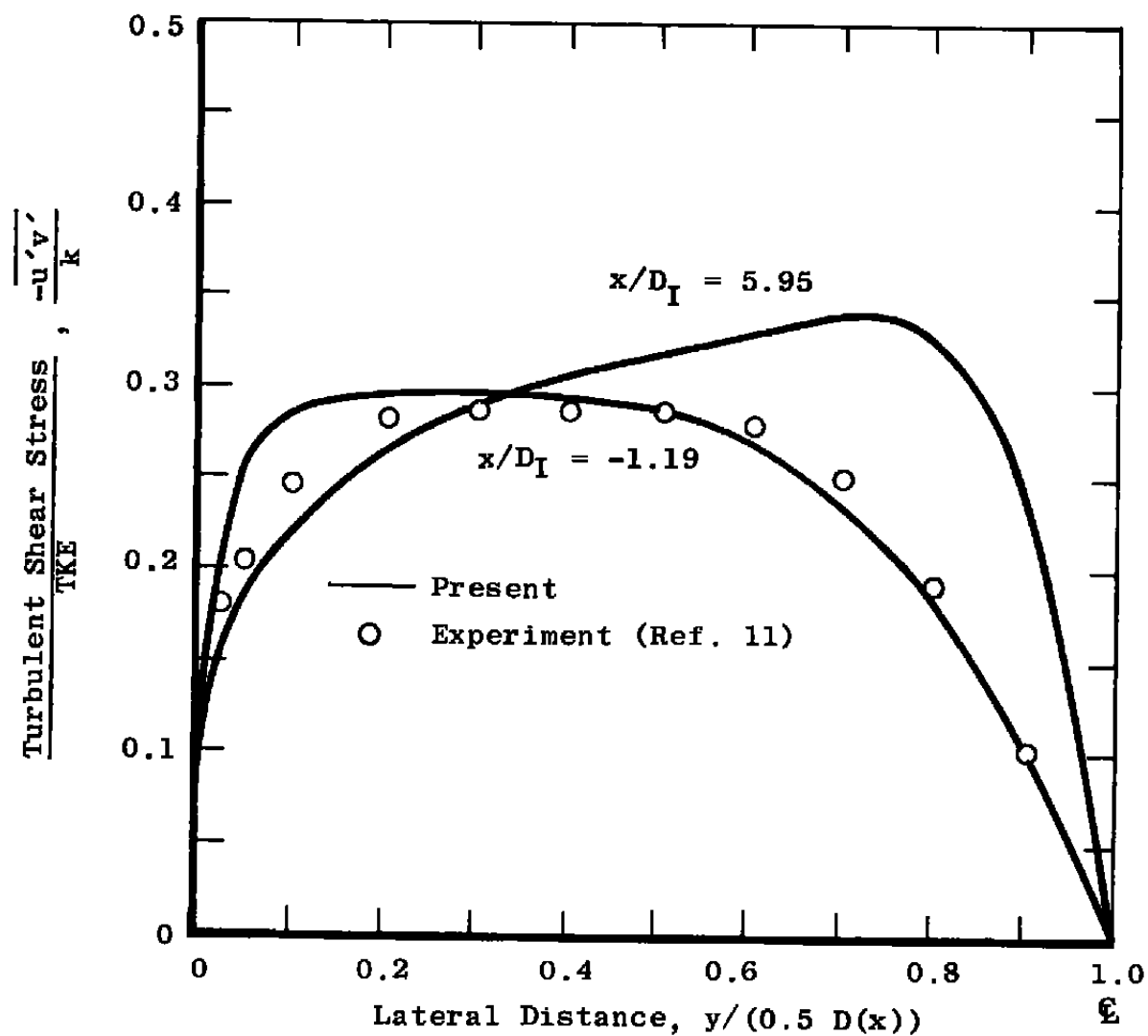**Figure 15. Turbulent kinetic energy distributions near the wall in 8-day conical diffuser.**

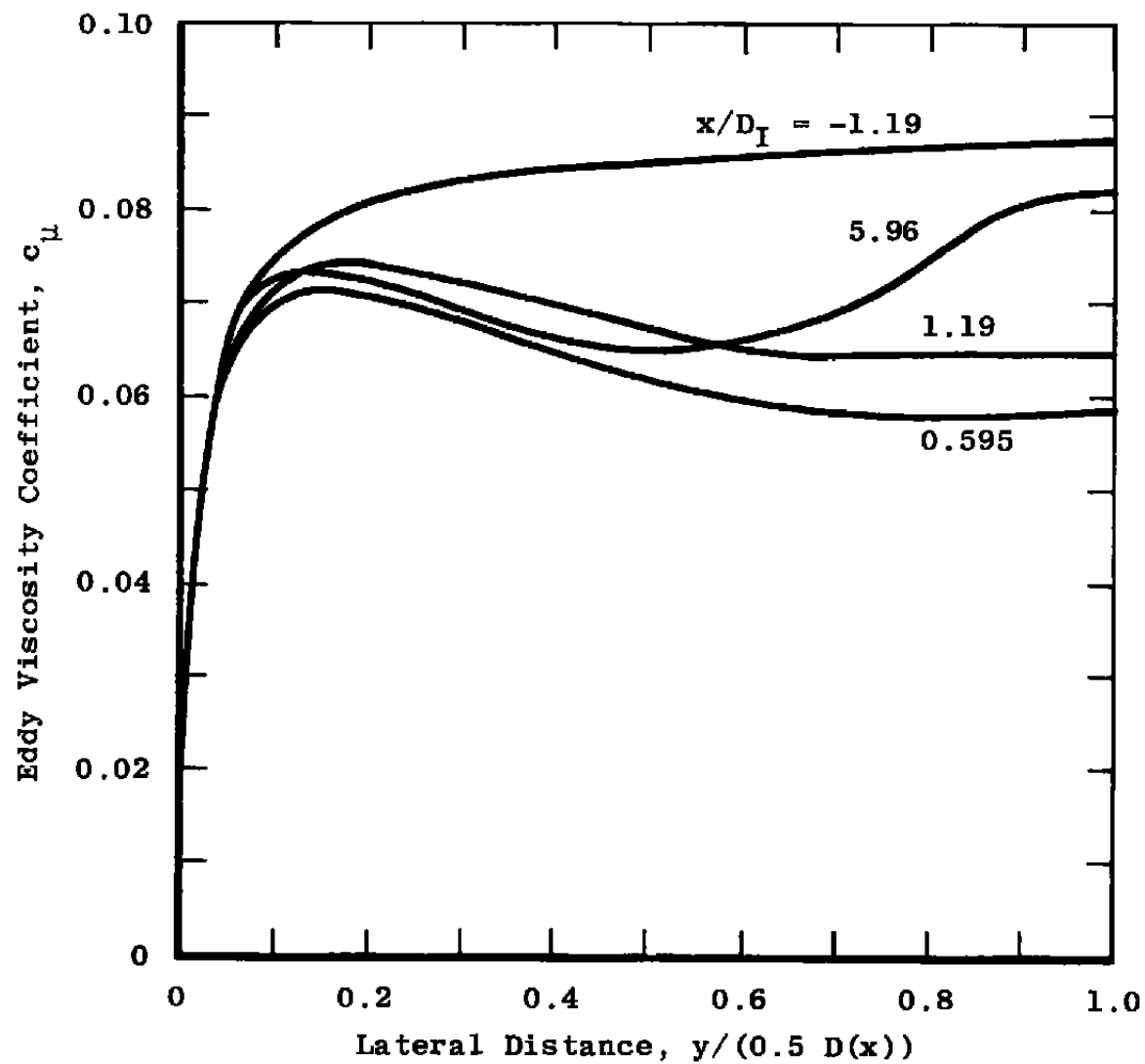Figure 16. Turbulent shear stress-TKE ratio in 8-deg conical diffuser.

Figure 17. Distributions of the eddy viscosity coefficient, c_μ, in 8-deg conical diffuser.
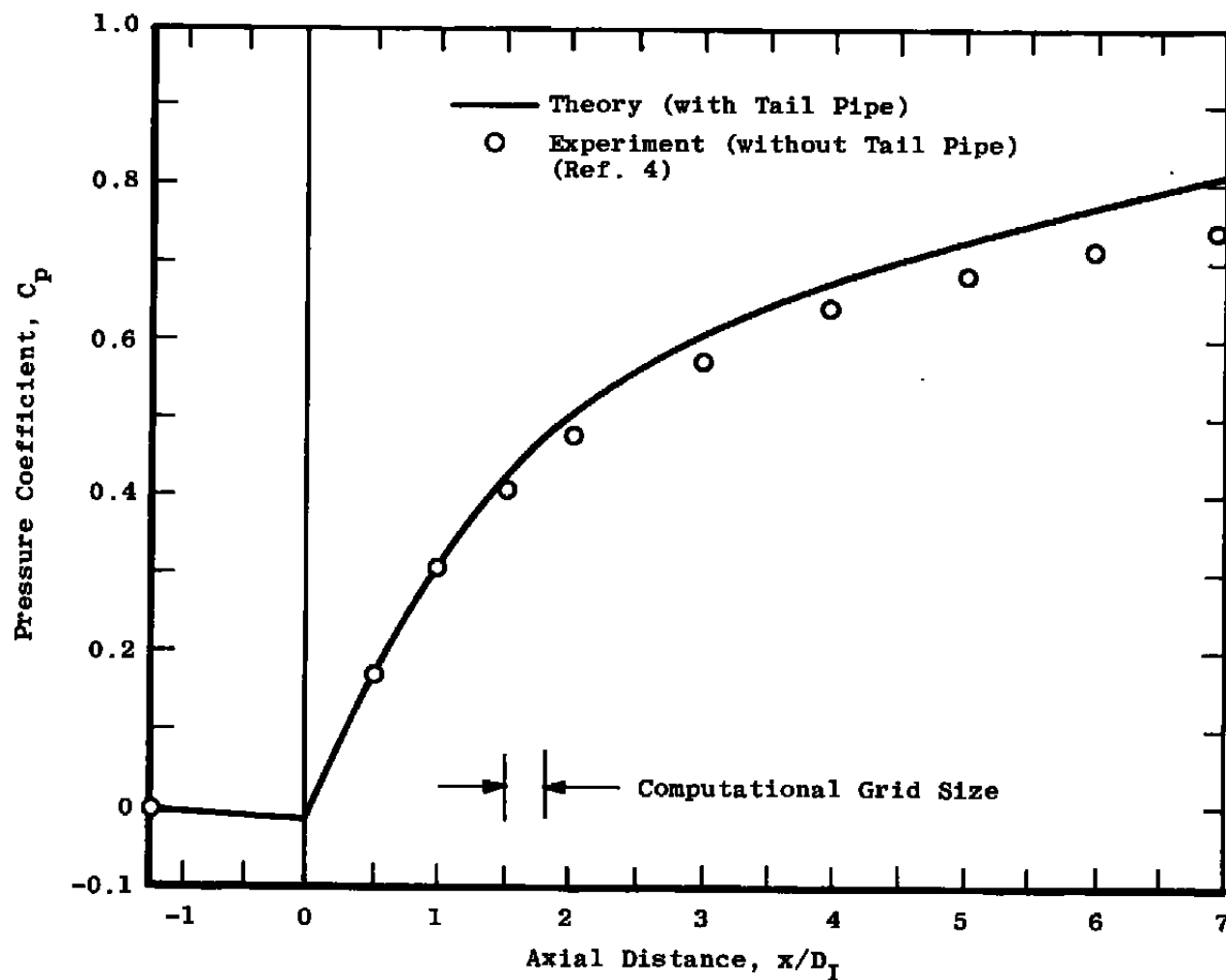
Figure 18. Pressure coefficient in 8-deg conical diffuser with fully developed inlet profile.

Figure 19. Velocity distribution in 8-deg conical diffuser with a
boundary-layer inlet profile, $\delta_I = 0.05\ D_I$.

Figure 20. Pressure coefficient in 8-deg conical diffuser
with a boundary-layer inlet profile, $\delta_I = 0.05\ D_I$.

Figure 21. Velocity distributions in 8-deg conical diffuser with
a boundary-layer inlet profile, $\delta_I = 0.2\ D_I$.
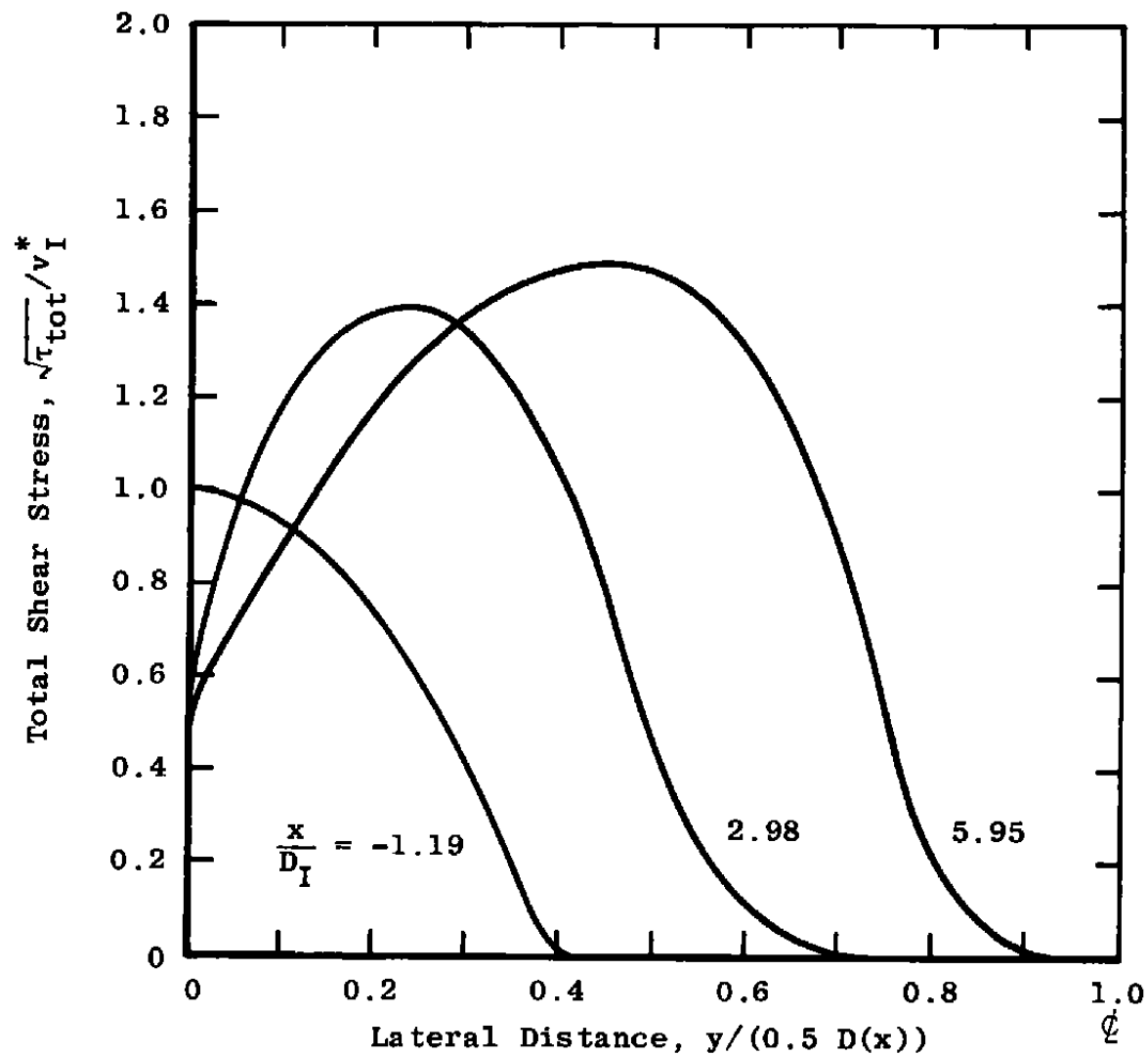
Figure 22.   Total shear stress distributions in 8-deg conical diffuser
with a boundary-layer inlet profile, $\delta_I = 0.2\ D_I$.
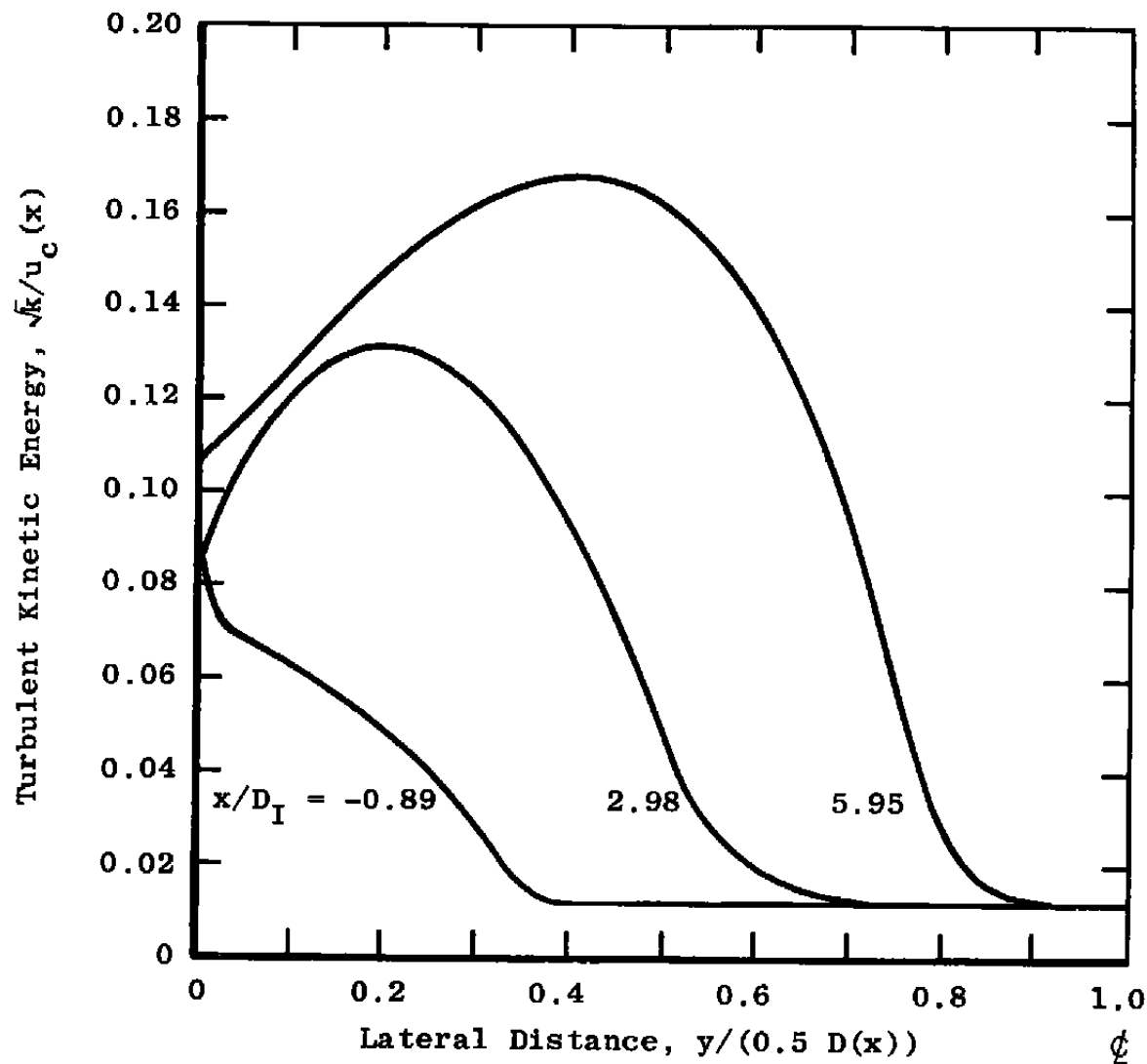
Figure 23. Turbulent kinetic energy distribution in 8-deg conical diffuser
with a boundary-layer inlet profile, δ_I = 0.2 D_I.
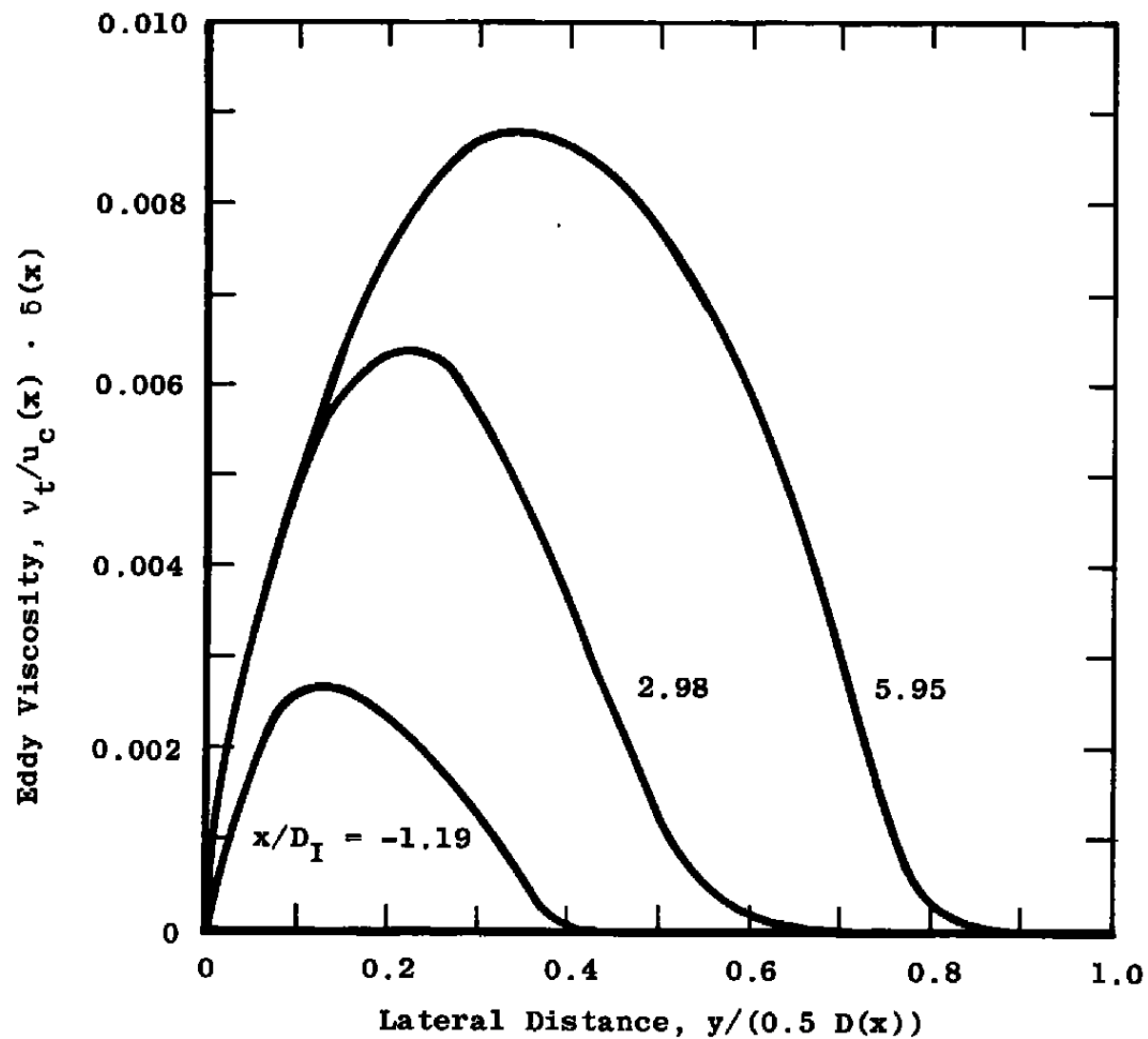
Figure 24. Eddy viscosity distributions in 8-deg conical diffuser with
a boundary-layer inlet condition, $\delta_I = 0.2\ D_I$.
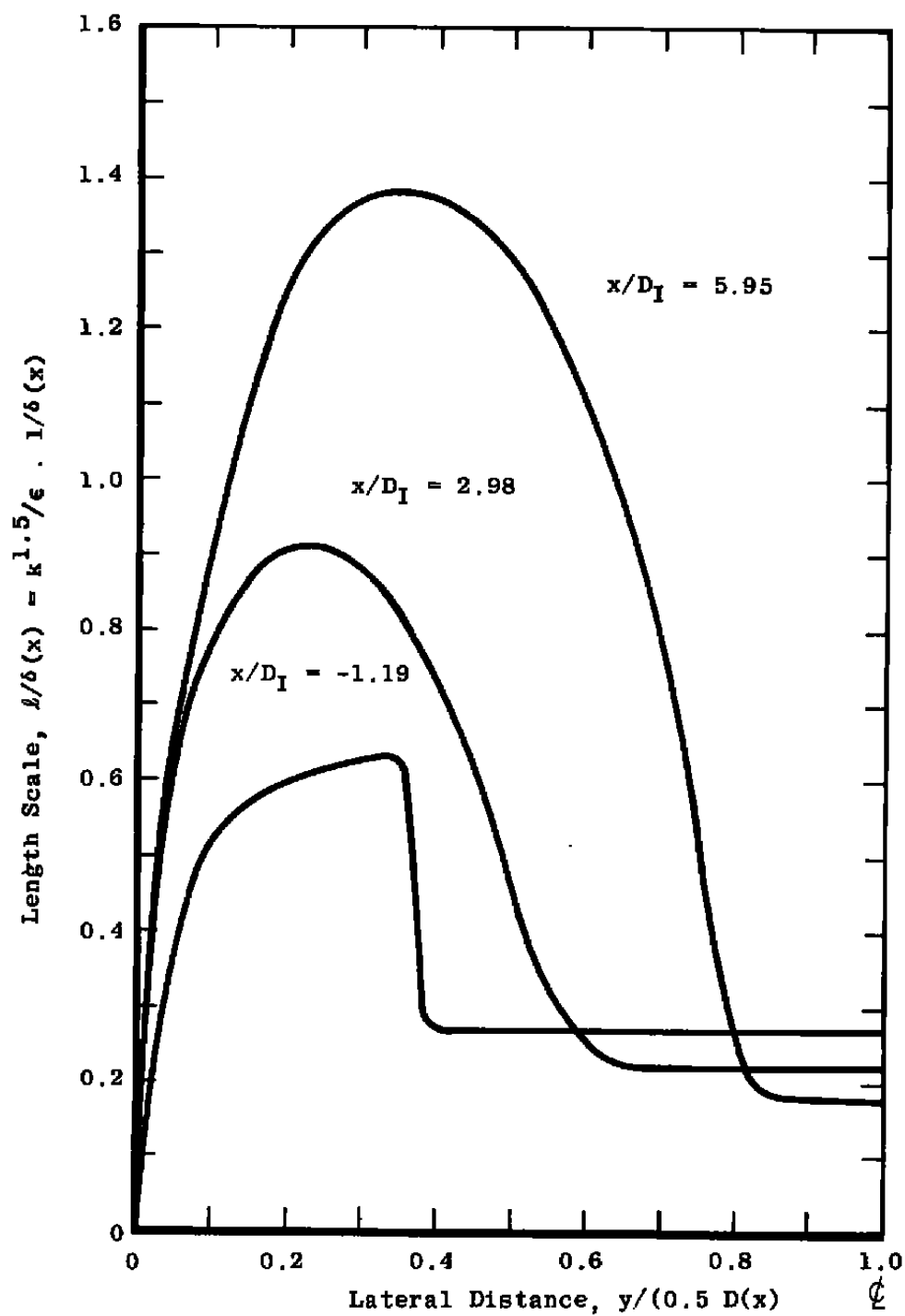
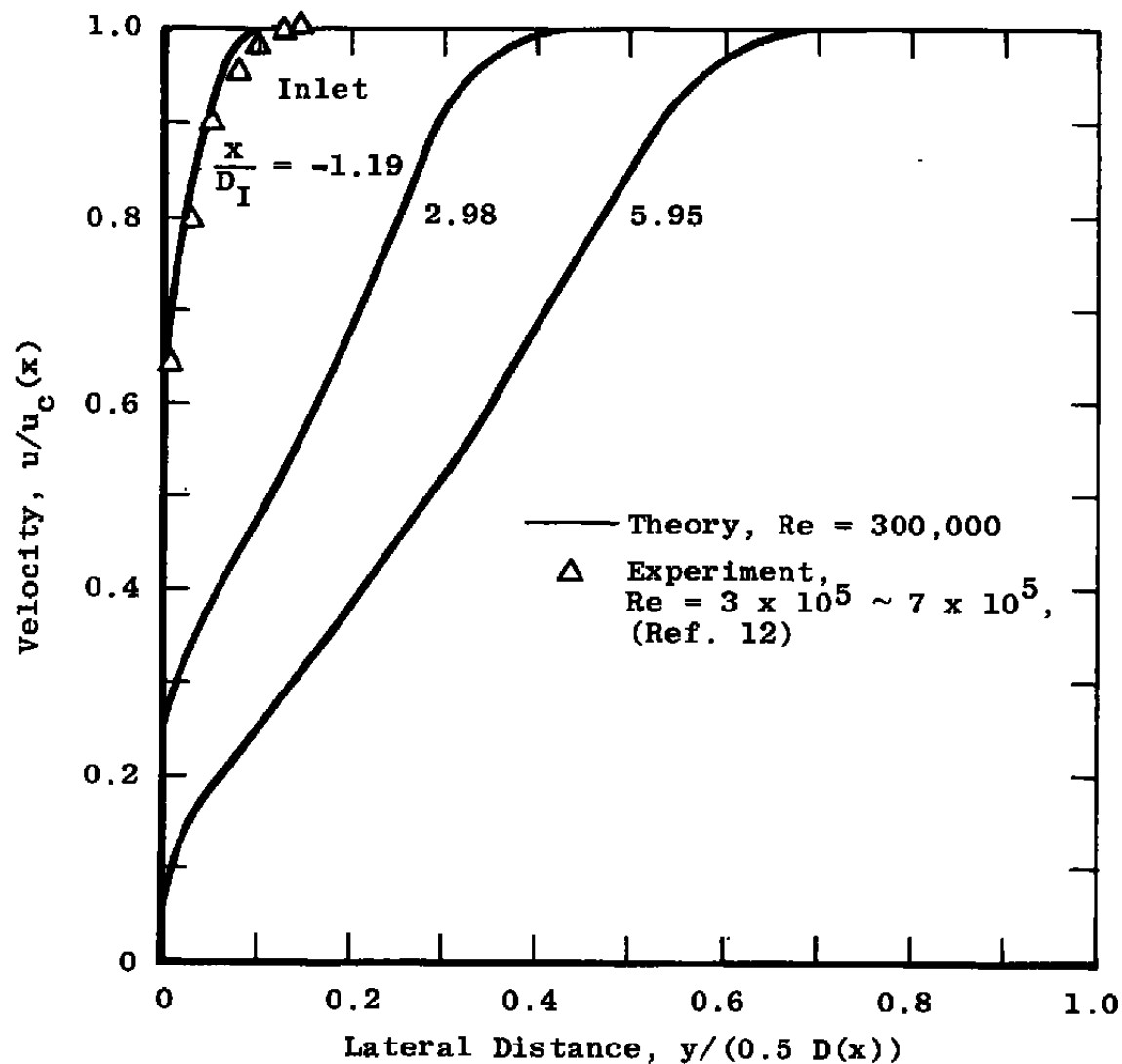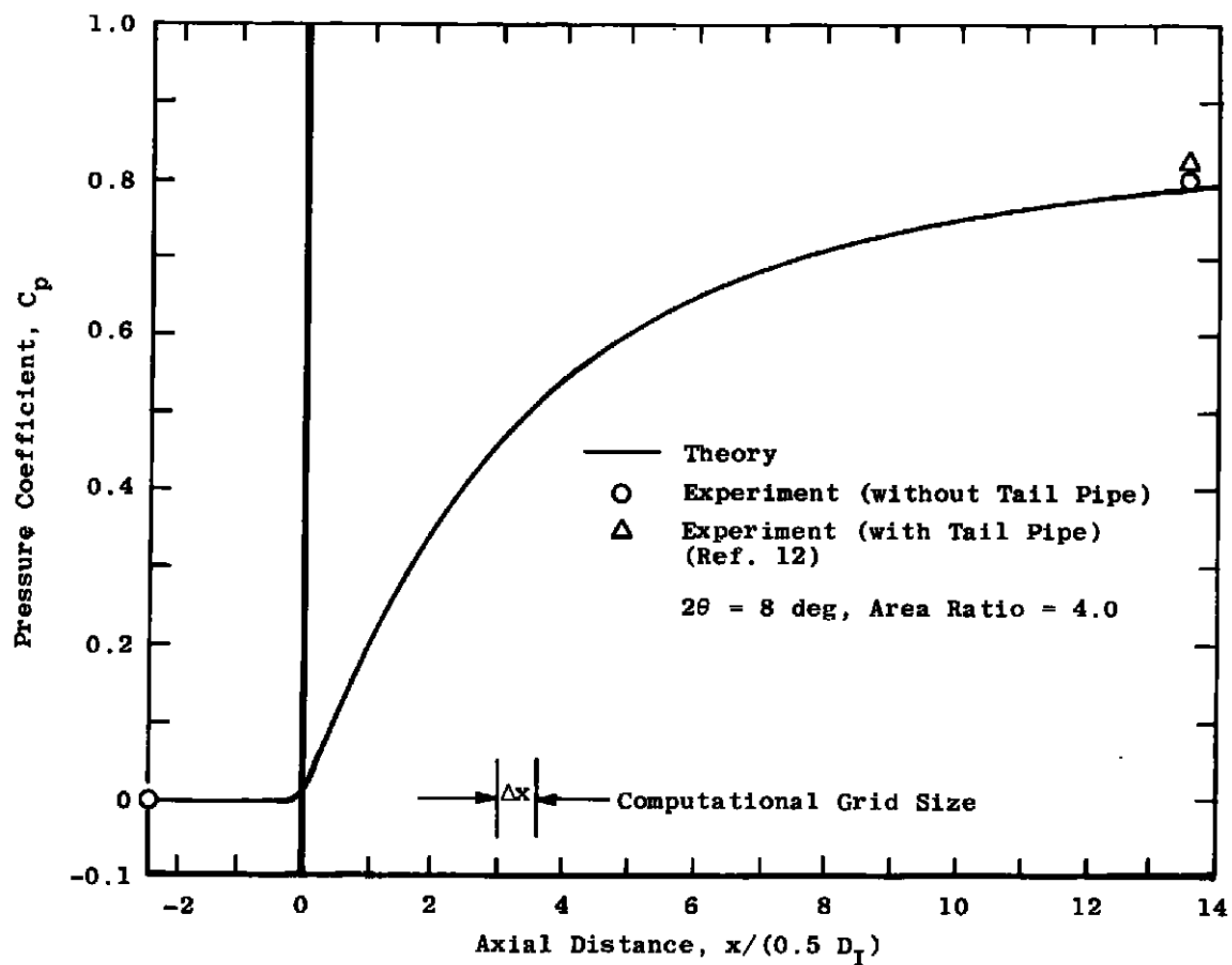Figure 25. Length scale distributions in 8-deg conical diffuser with a boundary-layer inlet condition, $\delta_I = 0.2\ D_I$.

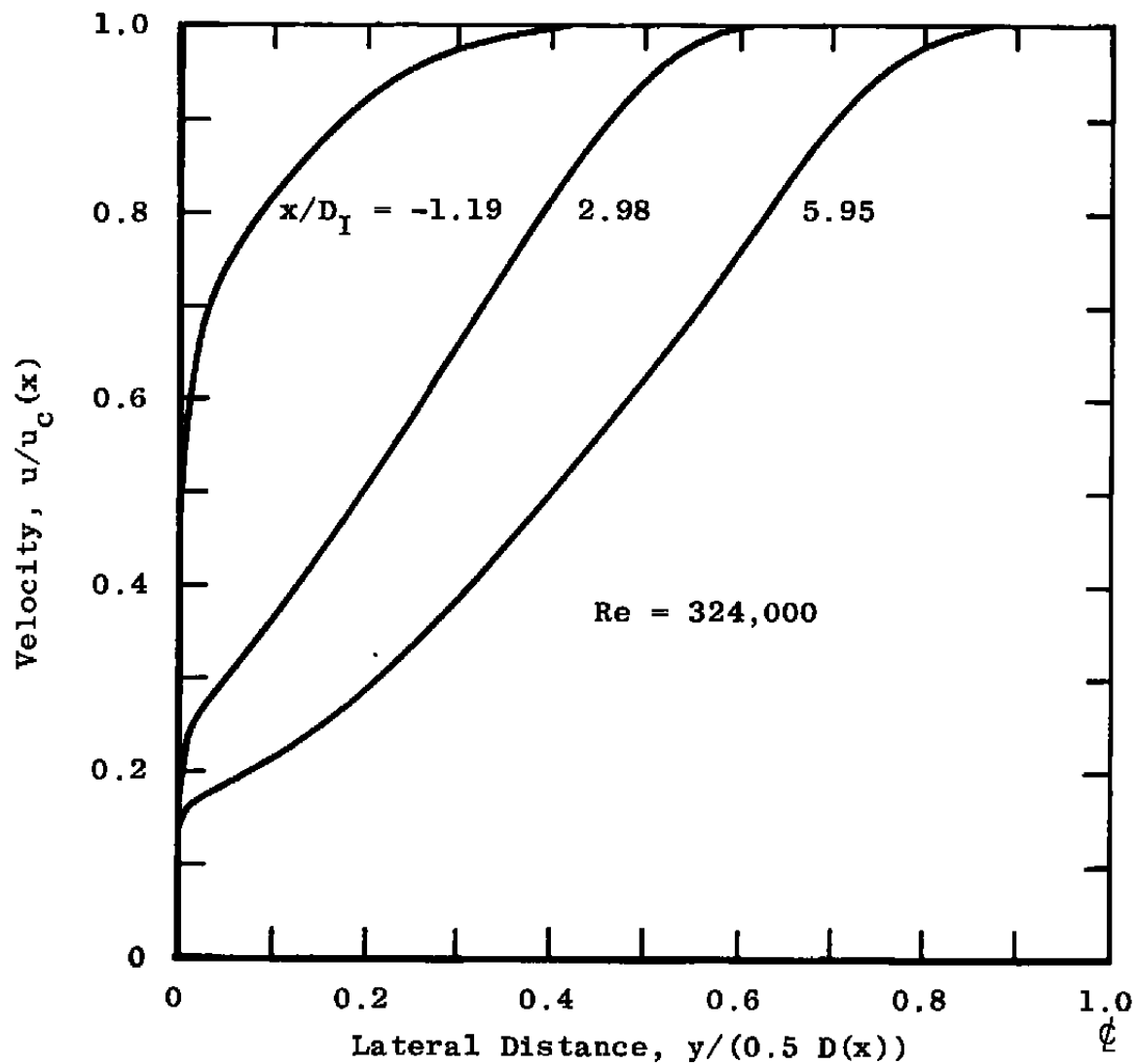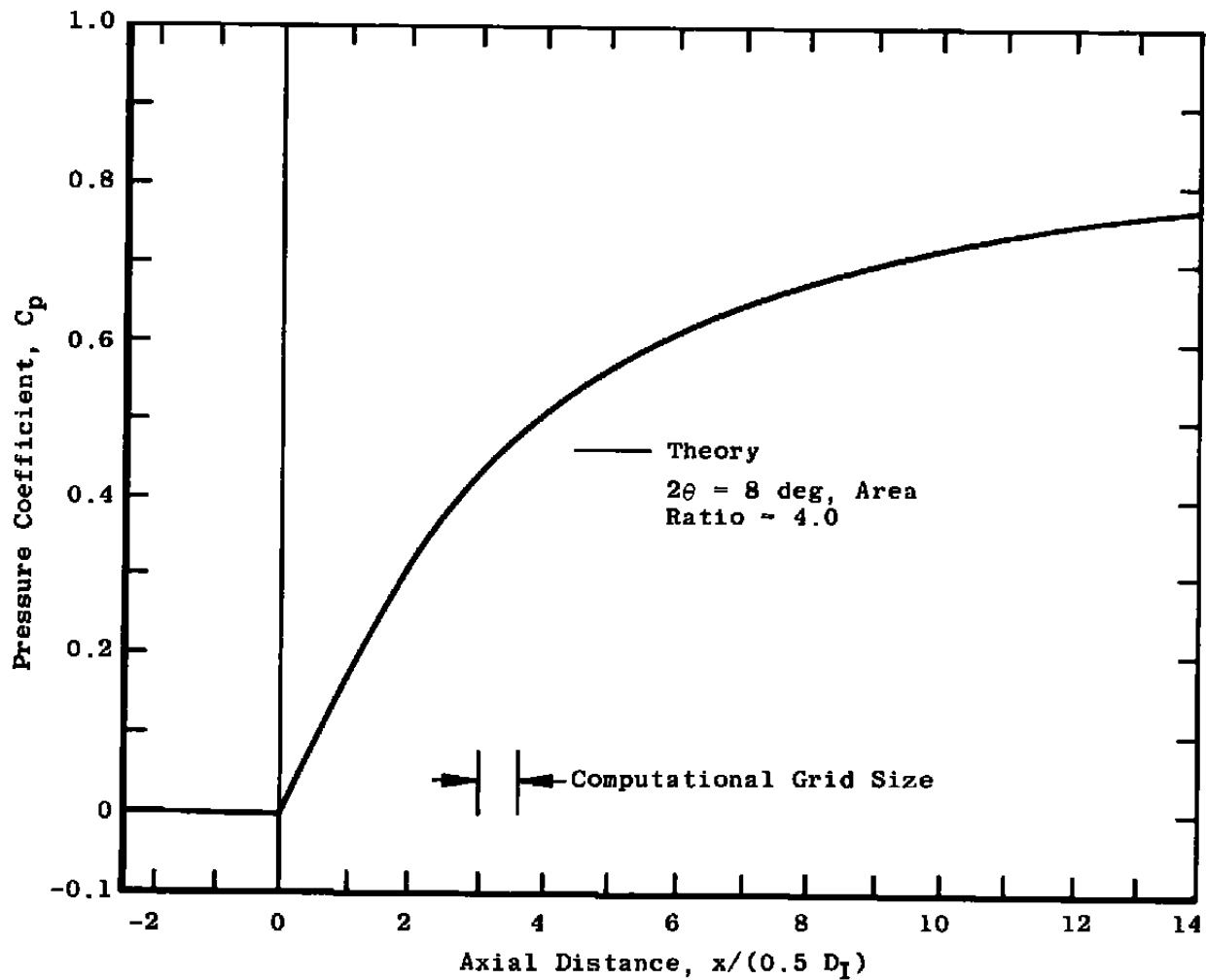Figure 26. Pressure coefficient in 8-deg conical diffuser with a boundary-layer inlet profile, $\delta_I = 0.2\ D_I$.
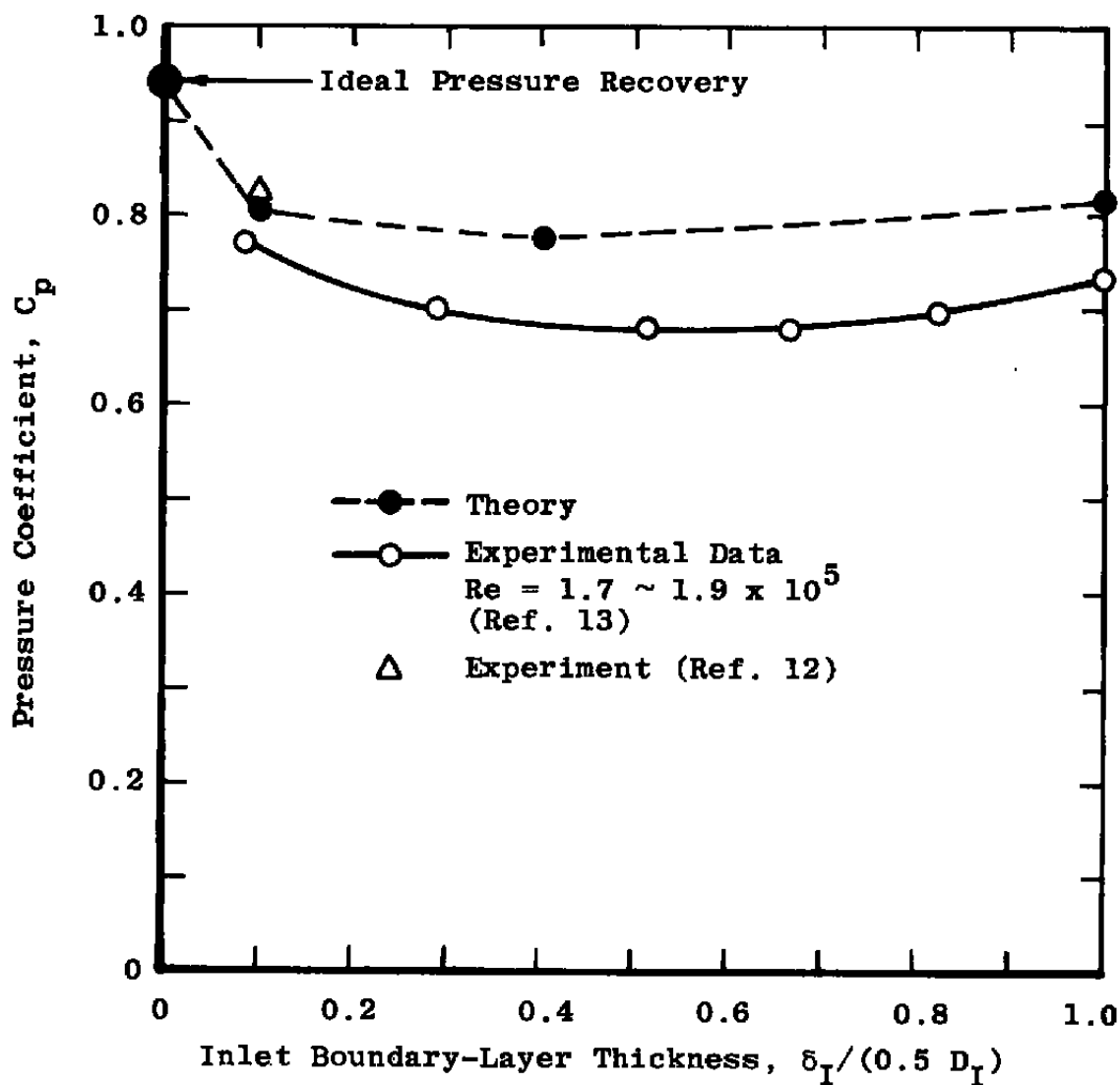
Figure 27. Effect of inlet boundary-layer thickness on the pressure recovery coefficient for 8-deg conical diffuser.

Figure 28. Velocity distributions in 16-deg conical diffuser with
a boundary-layer inlet profile.

Figure 29. Pressure coefficient in 16-deg conical diffuser
with a boundary-layer inlet condition.

Figure 30. Velocity distributions in 13-deg conical diffuser
with a boundary-layer inlet condition.

Figure 31. Pressure coefficient for a 13-deg conical diffuser with
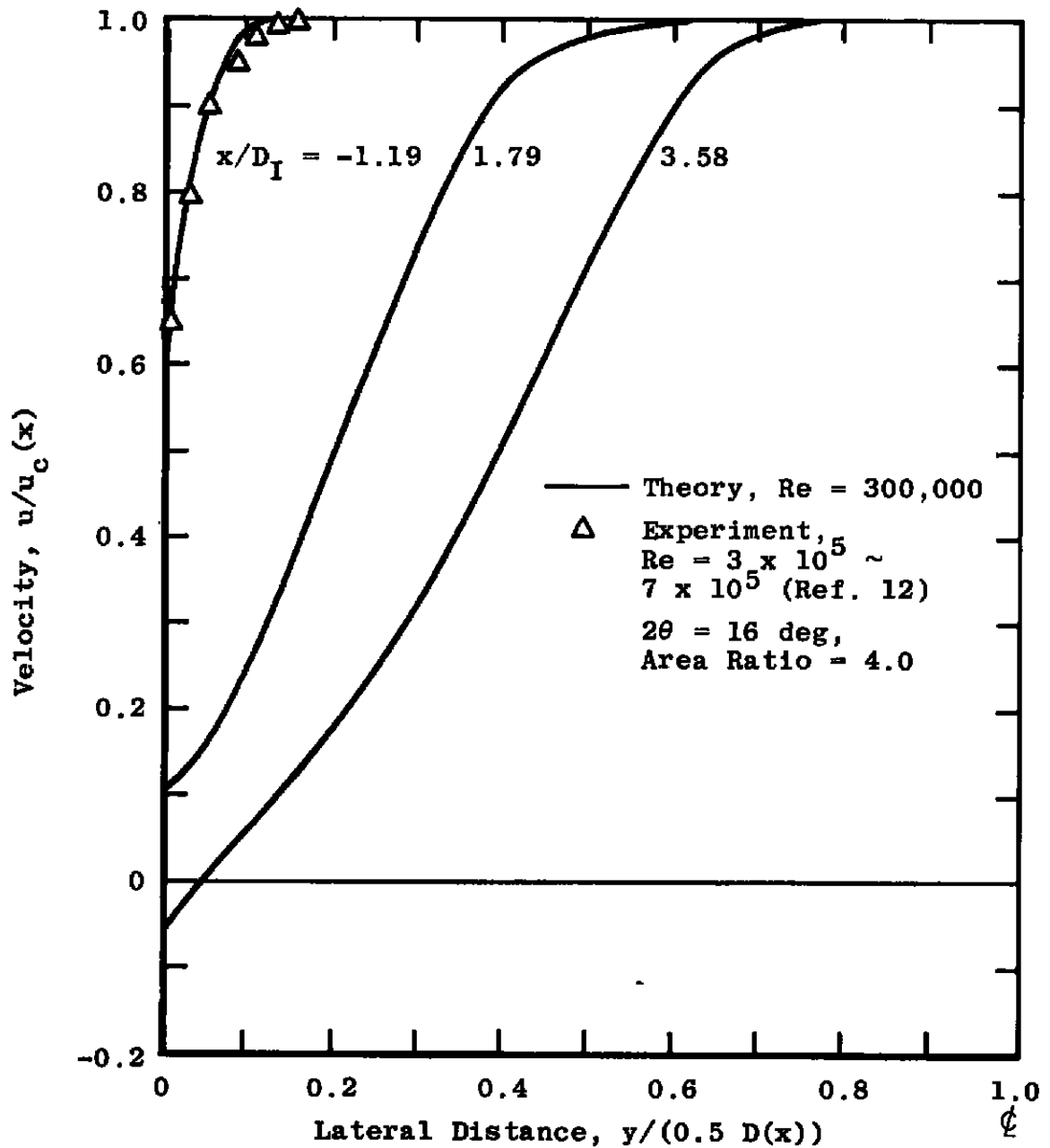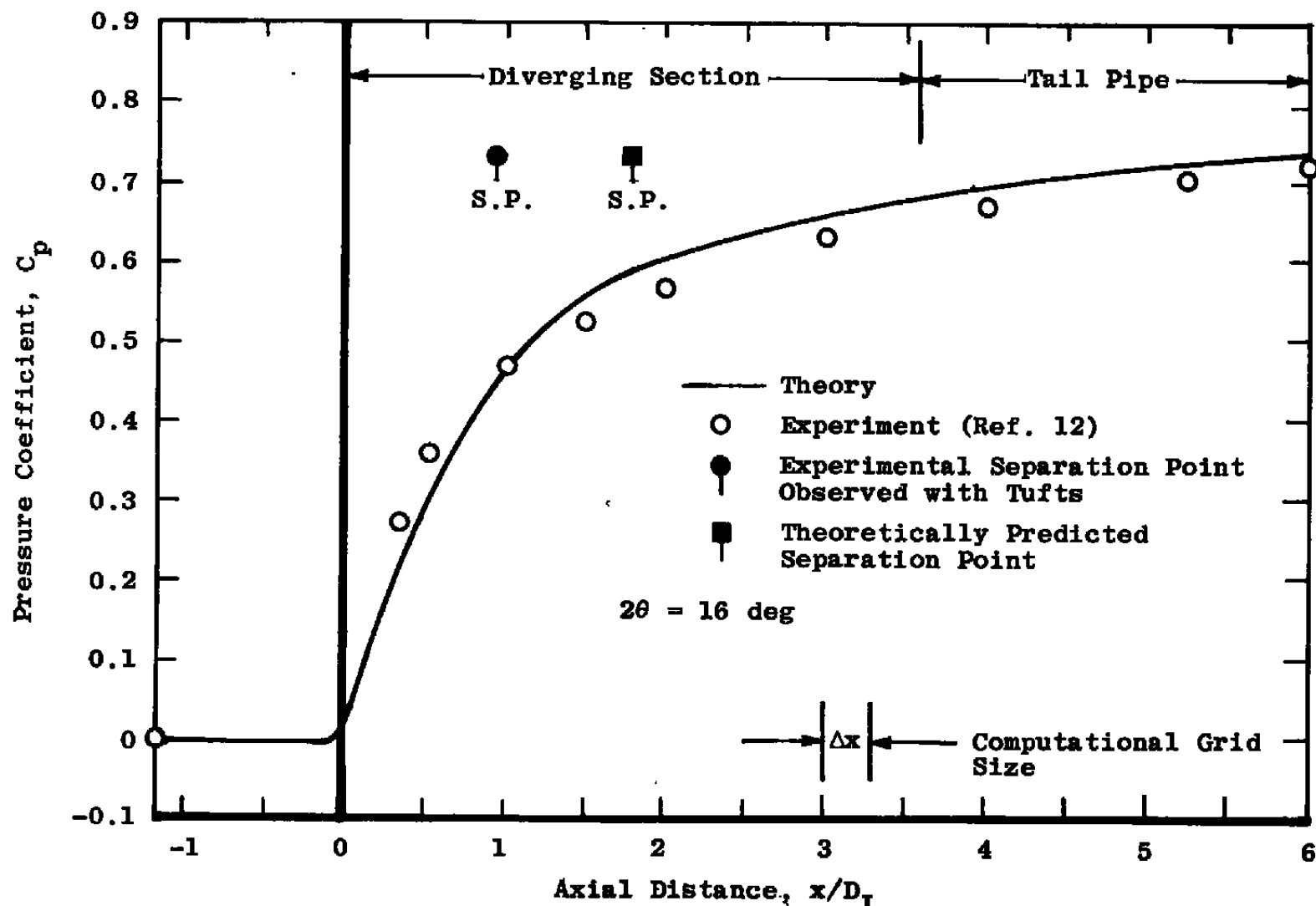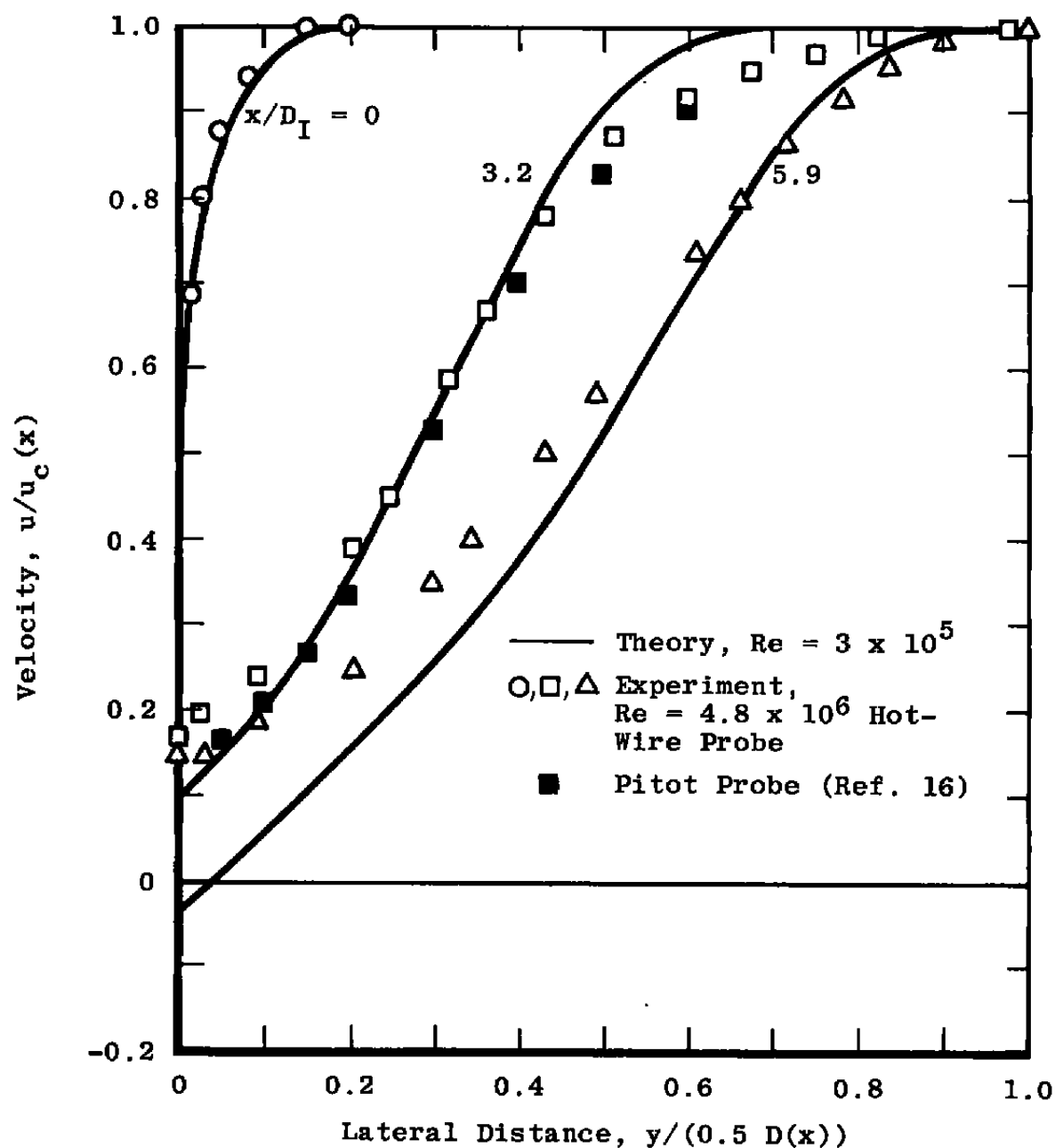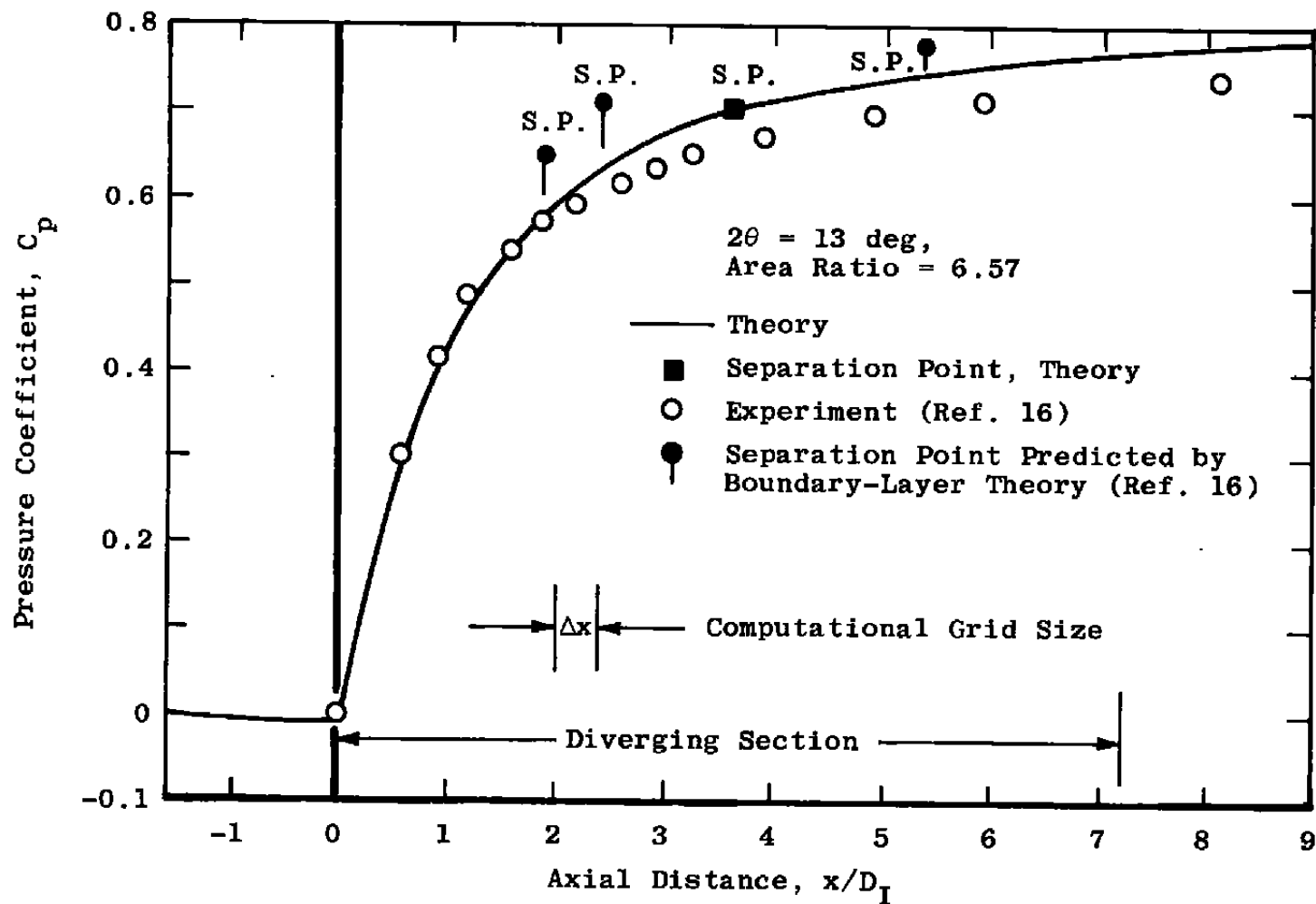a boundary-layer inlet profile.

APPENDIX A
GOVERNING EQUATIONS IN TRANSFORMED COORDINATES

The standard form of the derived equations, Ref. 1, is

$$\left\{ a_1 \frac{\partial^2 \phi}{\partial \bar{x}^2} + a_2 \frac{\partial^2 \phi}{\partial \bar{r}^2} \right\} - \left\{ b_1 \frac{\partial \phi}{\partial \bar{x}} + b_2 \frac{\partial \phi}{\partial \bar{r}} \right\} + d = 0 \tag{A-1}$$

where ϕ represents the flow variables, i.e., Ω, Ψ, k, and ε. The corresponding coefficients, a_1, a_2, b_1, b_2, and d are given below for each of variable, Ω, Ψ, k, and ε.

Ω-Equation

$$a_1 = 1$$

$$a_2 = \left[\left(\frac{\partial \bar{r}}{\partial x} \right)^2 + \left(\frac{\partial \bar{r}}{\partial r} \right)^2 \right]$$

$$b_1 = \frac{1}{(\nu + \nu_t)} \left\{ u - 2 \left[\frac{\partial \nu_t}{\partial \bar{x}} + \left(\frac{\partial \bar{r}}{\partial x} \right) \frac{\partial \nu_t}{\partial \bar{r}} \right] \right\}$$

$$b_2 = \frac{1}{(\nu + \nu_t)} \left\{ \left[v - 2 \left(\frac{\partial \bar{r}}{\partial r} \right) \frac{\partial \nu_t}{\partial \bar{r}} - \frac{\delta}{r} (\nu + \nu_t) \right] \left(\frac{\partial \bar{r}}{\partial r} \right) \right.$$
$$\left. + \left[u - 2 \left[\frac{\partial \nu_t}{\partial \bar{x}} + \left(\frac{\partial \bar{r}}{\partial x} \right) \frac{\partial \nu_t}{\partial \bar{r}} \right] \right] \left(\frac{\partial \bar{r}}{\partial x} \right) - (\nu + \nu_t) \left[\left(\frac{\partial^2 \bar{r}}{\partial x^2} \right) + \left(\frac{\partial^2 \bar{r}}{\partial r^2} \right) \right] \right\}$$

$$d = 2 \left(\frac{\partial \bar{r}}{\partial x} \right) \frac{\partial^2 \Psi}{\partial \bar{x} \partial \bar{r}} + \delta \left\{ \frac{v}{r} + \frac{1}{r} \left(\frac{\partial \bar{r}}{\partial r} \right) \frac{\partial \nu_t}{\partial \bar{r}} - \frac{(\nu - \nu_t)}{r^2} \right\} \frac{\Omega}{(\nu + \nu_t)}$$

$$+ \frac{1}{(\nu - \nu_t)} \left\{ \frac{\partial^2 \nu_t}{\partial \bar{x}^2} \left[\frac{\partial u}{\partial \bar{r}} \left(\frac{\partial \bar{r}}{\partial r} \right) + \frac{\partial v}{\partial \bar{x}} + \left(\frac{\partial \bar{r}}{\partial x} \right) \frac{\partial v}{\partial \bar{r}} \right] \right. \tag{A-2}$$

$$+ \frac{\partial^2 \nu_t}{\partial \bar{r}^2} \left\{ \left[\left(\frac{\partial \bar{r}}{\partial x} \right)^2 - \left(\frac{\partial \bar{r}}{\partial r} \right)^2 \right] \left[\frac{\partial u}{\partial \bar{r}} \left(\frac{\partial \bar{r}}{\partial r} \right) + \frac{\partial v}{\partial \bar{x}} + \left(\frac{\partial \bar{r}}{\partial x} \right) \frac{\partial v}{\partial \bar{r}} \right] \right.$$

$$\left. + 2 \left(\frac{\partial \bar{r}}{\partial r} \right) \left(\frac{\partial \bar{r}}{\partial x} \right) \left[\frac{\partial v}{\partial \bar{r}} \left(\frac{\partial \bar{r}}{\partial r} \right) - \left(\frac{\partial u}{\partial x} \right) - \left(\frac{\partial \bar{r}}{\partial x} \right) \frac{\partial u}{\partial \bar{r}} \right] \right\}$$

$$+ \frac{\partial^2 \nu_t}{\partial \bar{r}^2} \left\{ \left(\frac{\partial^2 \bar{r}}{\partial x^2} - \frac{\partial^2 \bar{r}}{\partial r^2} \right) \left[\frac{\partial u}{\partial \bar{r}} \left(\frac{\partial \bar{r}}{\partial r} \right) + \frac{\partial v}{\partial \bar{x}} + \left(\frac{\partial \bar{r}}{\partial x} \right) \frac{\partial v}{\partial \bar{r}} \right] \right.$$

$$\left. + 2 \left(\frac{\partial^2 \bar{r}}{\partial x \partial r} \right) \left[\frac{\partial v}{\partial \bar{r}} \left(\frac{\partial \bar{r}}{\partial r} \right) - \left(\frac{\partial u}{\partial \bar{x}} \right) - \left(\frac{\partial \bar{r}}{\partial x} \right) \frac{\partial u}{\partial \bar{r}} \right] \right\}$$

$$+ \frac{\partial^2 \nu_t}{\partial \bar{x} \partial \bar{r}} \left\{ 2 \left(\frac{\partial \bar{r}}{\partial x} \right) \left[\frac{\partial u}{\partial \bar{r}} \left(\frac{\partial \bar{r}}{\partial r} \right) + \frac{\partial v}{\partial \bar{x}} + \left(\frac{\partial \bar{r}}{\partial x} \right) \frac{\partial v}{\partial \bar{r}} \right] \right.$$

$$\left. \left. + 2 \left(\frac{\partial \bar{r}}{\partial r} \right) \left[\frac{\partial v}{\partial \bar{r}} \left(\frac{\partial \bar{r}}{\partial r} \right) - \left[\frac{\partial u}{\partial \bar{x}} + \left(\frac{\partial \bar{r}}{\partial x} \right) \frac{\partial u}{\partial \bar{r}} \right] \right] \right\} \right\}$$

Ψ-Equation

$$a_1 = 1$$

$$a_2 = \left[\left(\frac{\partial \tilde{r}}{\partial x}\right)^2 - \left(\frac{\partial \tilde{r}}{\partial r}\right)^2\right]$$

$$b_1 = 0$$

$$b_2 = -\frac{\partial^2 \tilde{r}}{\partial x^2} - \frac{\partial^2 \tilde{r}}{\partial r^2} + \frac{\delta}{r}\left(\frac{\partial \tilde{r}}{\partial r}\right)$$

$$d = 2\frac{\partial^2 \Psi}{\partial \tilde{x} \partial \tilde{r}}\left(\frac{\partial \tilde{r}}{\partial x}\right) + r^\delta \Omega$$

(A-3)

k-Equation

$$a_1 = 1$$

$$a_2 = \left[\left(\frac{\partial \tilde{r}}{\partial x}\right)^2 + \left(\frac{\partial \tilde{r}}{\partial r}\right)^2\right]$$

$$b_1 = \left\{u - \left[\frac{\partial \nu_t}{\partial \tilde{x}} + \left(\frac{\partial \tilde{r}}{\partial x}\right)\frac{\partial \nu_t}{\partial \tilde{r}}\right]\right\}\frac{1}{(\nu + \nu_t)}$$

$$b_2 = \frac{1}{(\nu + \nu_t)}\left\{\left[v - \left(\frac{\partial \tilde{r}}{\partial r}\right)\frac{\partial \nu_t}{\partial \tilde{r}} - \frac{\delta}{r}(\nu + \nu_t)\right]\left(\frac{\partial \tilde{r}}{\partial r}\right)\right.$$

$$\left. + \left[u - \left(\frac{\partial \nu_t}{\partial \tilde{x}} + \left(\frac{\partial \tilde{r}}{\partial x}\right)\frac{\partial \nu_t}{\partial \tilde{r}}\right)\right]\left(\frac{\partial \tilde{r}}{\partial x}\right) - (\nu + \nu_t)\left[\left(\frac{\partial^2 \tilde{r}}{\partial x^2}\right) + \left(\frac{\partial^2 \tilde{r}}{\partial r^2}\right)\right]\right\}$$

(A-4)

$$d = 2\left(\frac{\partial \tilde{r}}{\partial x}\right)\frac{\partial^2 k}{\partial \tilde{x} \partial \tilde{r}} + \left\{2\left[\left(\frac{\partial u}{\partial \tilde{x}} + \left(\frac{\partial \tilde{r}}{\partial x}\right)\frac{\partial u}{\partial \tilde{r}}\right)^2 + \left[\frac{\partial v}{\partial \tilde{r}}\left(\frac{\partial \tilde{r}}{\partial r}\right)\right]^2 + \delta\left(\frac{v}{r}\right)^2\right]\right.$$

$$+ \left[\frac{\partial u}{\partial \tilde{r}}\left(\frac{\partial \tilde{r}}{\partial r}\right) + \frac{\partial v}{\partial \tilde{x}} + \left(\frac{\partial \tilde{r}}{\partial x}\right)\frac{\partial v}{\partial \tilde{r}}\right]^2\right\}\frac{\nu_t}{(\nu + \nu_t)} - \frac{1}{(\nu + \nu_t)}\left\{\frac{c_\mu k}{\nu_t} + \frac{2\nu}{y^2}\right\}k$$

ε-Equation

$$a_1 = 1$$

$$a_2 = \left[\left(\frac{\partial \tilde{r}}{\partial x}\right)^2 + \left(\frac{\partial \tilde{r}}{\partial r}\right)^2\right]$$

$$b_1 = \frac{1}{(\nu - \nu_t/\sigma_\epsilon)}\left\{u - \left[\frac{\partial}{\partial \tilde{x}}\left(\frac{\nu_t}{\sigma_\epsilon}\right) + \left(\frac{\partial \tilde{r}}{\partial x}\right)\frac{\partial}{\partial \tilde{r}}\left(\frac{\nu_t}{\sigma_\epsilon}\right)\right]\right\}$$

$$b_2 = \frac{1}{(\nu + \nu_t/\sigma_\epsilon)}\left\{\left[v - \left(\frac{\partial \tilde{r}}{\partial r}\right)\frac{\partial}{\partial \tilde{r}}\left(\frac{\nu_t}{\sigma_\epsilon}\right) - \frac{\delta}{r}(\nu + \nu_t/\sigma_\epsilon)\right]\left(\frac{\partial \tilde{r}}{\partial r}\right)\right.$$

(A-5)

$$+ \left[u - \left(\frac{\partial}{\partial \tilde{x}}\left(\frac{\nu_t}{\sigma_\epsilon}\right) + \left(\frac{\partial \tilde{r}}{\partial x}\right)\frac{\partial}{\partial \tilde{r}}\left(\frac{\nu_t}{\sigma_\epsilon}\right)\right)\right]\left(\frac{\partial \tilde{r}}{\partial x}\right)$$

$$- (\nu + \nu_t/\sigma_\epsilon)\left[\left(\frac{\partial^2 \tilde{r}}{\partial x^2}\right) + \left(\frac{\partial^2 \tilde{r}}{\partial r^2}\right)\right]\right\}$$

68

$$d = 2\left(\frac{\partial \bar{r}}{\partial x}\right)\frac{\partial^2 \epsilon}{\partial \bar{x}\partial \bar{r}} + C_1 \frac{c_\mu k}{(\nu + \nu_t/\sigma_\epsilon)}\left\{2\left[\left(\frac{\partial u}{\partial \bar{x}} + \left(\frac{\partial \bar{r}}{\partial x}\right)\frac{\partial u}{\partial \bar{r}}\right)^2\right.\right.$$

$$+ \left[\frac{\partial v}{\partial \bar{r}}\left(\frac{\partial \bar{r}}{\partial r}\right)\right]^2 + \delta\left(\frac{v}{r}\right)^2\right] + \left[\frac{\partial u}{\partial \bar{r}}\left(\frac{\partial \bar{r}}{\partial r}\right) + \frac{\partial v}{\partial \bar{x}} + \left(\frac{\partial \bar{r}}{\partial x}\right)\frac{\partial v}{\partial \bar{r}}\right]^2\right\}$$

$$- C_2 \frac{\epsilon^2}{k}\frac{1}{(\nu + \nu_t/\sigma_\epsilon)}$$

In the vorticity-stream function formulation, the pressure field is decoupled from the momentum equations. Therefore, the pressure field can be calculated separately from the pressure equation. In the transformed plane, the pressure equation can be written as

$$\frac{\partial^2 p}{\partial \bar{x}^2} + \frac{\partial^2 p}{\partial \bar{r}^2}\cdot\left[\left(\frac{\partial \bar{r}}{\partial x}\right)^2 + \left(\frac{\partial \bar{r}}{\partial r}\right)^2\right]$$

$$+ \frac{\partial p}{\partial \bar{r}}\cdot\left[\left(\frac{\partial^2 \bar{r}}{\partial x^2}\right) + \left(\frac{\partial^2 \bar{r}}{\partial r^2}\right) + \frac{\delta}{r}\left(\frac{\partial \bar{r}}{\partial r}\right)\right] + 2\left(\frac{\partial \bar{r}}{\partial x}\right)\frac{\partial^2 p}{\partial \bar{x}\partial \bar{r}} = S_p \qquad (A\text{-}6)$$

where

$$S_p = \Omega^2 - \left\{\frac{\partial^2}{\partial \bar{x}^2}\left(\frac{v^2 + u^2}{2}\right) + \frac{\partial^2}{\partial \bar{r}^2}\left(\frac{v^2 + u^2}{2}\right)\cdot\left[\left(\frac{\partial \bar{r}}{\partial x}\right)^2 + \left(\frac{\partial \bar{r}}{\partial r}\right)^2\right]\right.$$

$$+ \frac{\partial}{\partial \bar{r}}\left(\frac{v^2 + u^2}{2}\right)\cdot\left[\left(\frac{\partial^2 \bar{r}}{\partial x}\right) + \left(\frac{\partial^2 \bar{r}}{\partial r^2}\right) + \frac{\delta}{r}\cdot\left(\frac{\partial \bar{r}}{\partial r}\right)\right] \qquad (A\text{-}7)$$

$$+ 2\left(\frac{\partial \bar{r}}{\partial x}\right)\frac{\partial^2}{\partial \bar{x}\partial \bar{r}}\left(\frac{v^2 + u^2}{2}\right)\Bigg\}$$

$$- u\frac{\partial \Omega}{\partial \bar{r}}\cdot\left(\frac{\partial \bar{r}}{\partial r}\right) - \delta u\frac{\Omega}{r} + v\frac{\partial \Omega}{\partial \bar{x}} + v\left(\frac{\partial \bar{r}}{\partial x}\right)\frac{\partial \Omega}{\partial \bar{r}}$$

The corresponding coefficients for the pressure equation in the standard form are:

$$a_1 = 1$$

$$a_2 = \left[\left(\frac{\partial \bar{r}}{\partial x}\right)^2 + \left(\frac{\partial \bar{r}}{\partial r}\right)^2\right]$$

$$b_1 = 0$$

$$b_2 = -\left[\left(\frac{\partial^2 \bar{r}}{\partial x^2}\right) + \left(\frac{\partial^2 \bar{r}}{\partial r^2}\right) + \frac{\delta}{r}\left(\frac{\partial \bar{r}}{\partial r}\right)\right] \qquad (A\text{-}8)$$

$$\cdot \, d = 2\left(\frac{\partial \bar{r}}{\partial x}\right)\frac{\partial^2 p}{\partial \bar{x}\partial \bar{r}} - \Omega^2 + \left\{\frac{\partial^2}{\partial \bar{x}}\left(\frac{v^2 + u^2}{2}\right) - \frac{\partial^2}{\partial \bar{r}}\left(\frac{v^2 + u^2}{2}\right)\cdot\left[\left(\frac{\partial \bar{r}}{\partial x}\right)^2 + \left(\frac{\partial \bar{r}}{\partial r}\right)^2\right]\right.$$

$$\cdot \, + \frac{\partial}{\partial \bar{r}}\left(\frac{v^2 + u^2}{2}\right)\left[\left(\frac{\partial^2 \bar{r}}{\partial x^2}\right) + \left(\frac{\partial^2 \bar{r}}{\partial r^2}\right) + \frac{\delta}{r}\cdot\left(\frac{\partial \bar{r}}{\partial r}\right)\right] + 2\left(\frac{\partial \bar{r}}{\partial x}\right)\frac{\partial^2}{\partial \bar{x}\partial \bar{r}}\left(\frac{v^2 + u^2}{2}\right)\Bigg\}$$

$$- u\frac{\partial \Omega}{\partial \bar{r}}\left(\frac{\partial \bar{r}}{\partial r}\right) - \delta u\frac{\Omega}{r} + v\frac{\partial \Omega}{\partial \bar{x}} + v\left(\frac{\partial \bar{r}}{\partial x}\right)\frac{\partial \Omega}{\partial \bar{r}}$$

NOMENCLATURE

A   Parameter

a   Constant

a_1, a_2 Coefficients

b   Constant

b_1, b_2 Coefficients

C   Transformation coefficient

C_1, C_2 Coefficients

C_p Pressure Coefficient, $\dfrac{\Delta p}{0.5\,\rho \bar{u}_I^2}$

c_μ, $c_{\mu o}$, $c_{\mu 1}$ Eddy viscosity coefficients

Δc_μ Eddy viscosity coefficient correction for axisymmetric flow

D   Local diffuser diameter

d   Source term

F   Transformation parameter

f   Rodi's c_μ correction for axisymmetric jet

G_i, G_j Decay Functions

g	Transformation parameter
K	Constant in Schlichting's round jet theory
k	Turbulent kinetic energy
k1, k2	Proportionality constants for k and ν_t in potential core
ℓ	Length scale
n	Iteration number
p	Pressure
R	Parameter
Re	Reynolds number, $\dfrac{D_I \bar{u}_I}{\nu}$
R_I, R_J	Grid Reynolds number
$r, \tilde{r}$	Radial coordinate in physical and transformed plane, respectively
$\tilde{r}_{max}$	Diffuser wall coordinate in transformed plane
S(x), SO(x)	Diffuser wall coordinate in physical plane
$\bar{u}$	Average velocity
u,v	Velocity components
Δu	Velocity excess in Rodi's c_μ model

u', v', w'	Turbulent velocity components
u_b	Wake component of the velocity profile
$v*$	$\equiv \sqrt{\tau_w / \delta}$, Friction Velocity
x	Axial coordinate
y	Lateral distance measured from wall
YG	The width of a round jet in Rodi's c_μ model
α, β	Transformation parameters
δ	Index, zero for planar configuration, 1 for axisymmetric configurations, or incremental or boundary-layer thickness
ϵ	Turbulent kinetic energy dissipation
2θ	Total diffuser divergence angle
ν	Molecular viscosity
ν_t	Eddy viscosity
σ_ϵ	Constant
τ	Shear stress
ϕ	Dependent variable
ψ	Stream function

Ω	Vorticity
η	Similarity parameter for round jet
ρ	Density
λ	Constant

SUBSCRIPTS

c	Centerline
e	Edge of the boundary layer
I	Inlet section
max	Maximum
o	Sublayer, core region solution matching location
T, tot	Total
w	Wall

SUPERSCRIPTS

+	Dimensionless quantity with the sublayer scale